

UNCLASSIFIED

AD NUMBER

ADB076165

LIMITATION CHANGES

TO:

Approved for public release; distribution is unlimited.

FROM:

Distribution authorized to U.S. Gov't. agencies only; Test and Evaluation; AUG 1983. Other requests shall be referred to Arnold Engineering Development Center, Attn: DOS, Arnold AFS, TN 37389.

AUTHORITY

AEDC ltr, 15 Mar 1989

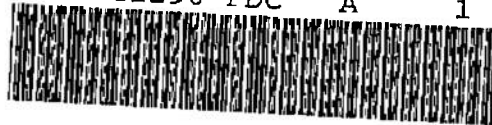
THIS PAGE IS UNCLASSIFIED

UNCLASSIFIED

AEDC-TR-83-26

Girata

DOC NUM SER CN
UNC11290-PDC A 1



Particle Sampling with Supersonic Probes

Similitude and Particle Breakup

L. J. Forney
Georgia Institute of Technology
Atlanta, Georgia 30332
and
W. K. McGregor and P. T. Girata, Jr.
Sverdrup Technology, Inc.

August 1983

Final Report for Period June 21 — September 10, 1982

Distribution limited to U.S. Government agencies only; this document contains information on test and evaluation of military hardware; August 1983; other requests for this document must be referred to Arnold Engineering Development Center/DOS, Arnold Air Force Station, Tennessee 37389.

SUBJECT TO EXPORT CONTROL LAWS

This document contains information for manufacturing or using munitions of war. Export of the information contained herein, or release to foreign nationals within the United States, without first obtaining an export license, is a violation of the International Traffic in Arms Regulations. Such violation is subject to a penalty of up to 2 years imprisonment and a fine of \$100,000 under 22 U.S.C. 2778. Include this notice with any reproduced portion of this document.

**ARNOLD ENGINEERING DEVELOPMENT CENTER
ARNOLD AIR FORCE STATION, TENNESSEE
AIR FORCE SYSTEMS COMMAND
UNITED STATES AIR FORCE**

UNCLASSIFIED

NOTICES

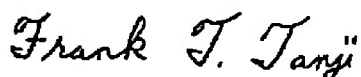
When U. S. Government drawings, specifications, or other data are used for any purpose other than a definitely related Government procurement operation, the Government thereby incurs no responsibility nor any obligation whatsoever, and the fact that the government may have formulated, furnished, or in any way supplied the said drawings, specifications, or other data, is not to be regarded by implication or otherwise, or in any manner licensing the holder or any other person or corporation, or conveying any rights or permission to manufacture, use, or sell any patented invention that may in any way be related thereto.

Qualified users may obtain copies of this report from the Defense Technical Information Center.

References to named commercial products in this report are not to be considered in any sense as an endorsement of the product by the United States Air Force or the Government.

APPROVAL STATEMENT

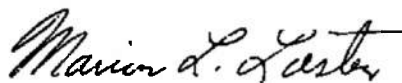
This report has been reviewed and approved.



FRANK T. TANJI, Captain, USAF
Directorate of Technology
Deputy for Operations

Approved for publication:

FOR THE COMMANDER



MARION L. LASTER
Director of Technology
Deputy for Operations

UNCLASSIFIED

SECURITY CLASSIFICATION OF THIS PAGE (When Data Entered)

REPORT DOCUMENTATION PAGE		READ INSTRUCTIONS BEFORE COMPLETING FORM
1. REPORT NUMBER AEDC-TR-83-26	2. GOVT ACCESSION NO.	3. RECIPIENT'S CATALOG NUMBER
4. TITLE (and Subtitle) PARTICLE SAMPLING WITH SUBSONIC PROBES: Similitude and Particle Breakup		5. TYPE OF REPORT & PERIOD COVERED Final Report, June 21 - September 10, 1982
		6. PERFORMING ORG. REPORT NUMBER
7. AUTHOR(s) L. J. Forney, Georgia Institute of Technology, and W. K. McGregor and P. T. Girata, Jr., Sverdrup Technology, Inc./AEDC Group		8. CONTRACT OR GRANT NUMBER(s)
9. PERFORMING ORGANIZATION NAME AND ADDRESS Arnold Engineering Development Center/DOT Air Force Systems Command Arnold Air Force Station, TN 37389		10. PROGRAM ELEMENT, PROJECT, TASK AREA & WORK UNIT NUMBERS Program Element 65807F
11. CONTROLLING OFFICE NAME AND ADDRESS Arnold Engineering Development Center/DOS Air Force Systems Command Arnold Air Force Station, TN 37389		12. REPORT DATE August 1983
		13. NUMBER OF PAGES 47
14. MONITORING AGENCY NAME & ADDRESS (if different from Controlling Office)		15. SECURITY CLASS. (of this report) UNCLASSIFIED
		15a. DECLASSIFICATION/DOWNGRADING SCHEDULE N/A
16. DISTRIBUTION STATEMENT (of this Report) Distribution limited to U.S. Government agencies only; this report contains information on test and evaluation of military hardware; August 1983; other requests for this document must be referred to Arnold Engineering Development Center/DOS, Arnold Air Force Station, Tennessee 37389.		
17. DISTRIBUTION STATEMENT (of the abstract entered in Block 20, if different from Report)		
18. SUPPLEMENTARY NOTES Available in Defense Technical Information Center (DTIC).		
19. KEY WORDS (Continue on reverse side if necessary and identify by block number) particle sampling supersonic particle probe particle breakup collection efficiency		
20. ABSTRACT (Continue on reverse side if necessary and identify by block number) Characteristics of the flow field, shock detachment, and particle trajec- tories are discussed for a cylindrical, supersonic particle probe. The form of the scaling law for probe collection efficiency is suggested for both Stokesian and non-Stokesian particles from the normalized equation of particle motion and simple expressions for the particle drag coefficient. Conditions for the onset of particle breakup in normal shock waves have been investigated. A normalized particle drag behind the shock has been determined in terms of gas stagnation conditions and particle diameter for a range of gas Mach numbers between 1 and		

UNCLASSIFIED

SECURITY CLASSIFICATION OF THIS PAGE (When Data Entered)

UNCLASSIFIED

SECURITY CLASSIFICATION OF THIS PAGE(When Data Entered)

20. ABSTRACT, Concluded.

5 by including appropriately defined particle Knudsen and Reynolds numbers in analytical expressions for the drag coefficient. Numerical computations of the particle drag, normalized with gas stagnation pressure and particle area, indicate a peak at a gas Mach number of about 2.2. The magnitude of the peak was found to decrease with increasing particle diameter and reservoir gas density. Criteria for the onset of agglomerate breakup were defined in terms of a modified Weber number for the adhesion mechanisms due to Van der Waals forces, electrostatic attraction, and adsorbed surface films. These results indicate that larger and more closely packed agglomerates made up of smaller constituent particles have a greater tendency to resist breakup for a given set of gas stagnation conditions and shock Mach number than do agglomerates containing fewer, but larger, constituent particles. These results are useful for the design of experiments to simulate the collection efficiency of particle sampling probes and in interpreting the data obtained from sampling of two-phase flows.

UNCLASSIFIED

SECURITY CLASSIFICATION OF THIS PAGE(When Data Entered)

PREFACE

The work reported herein was sponsored by the Air Force Office of Scientific Research (AFOSR), Air Force Systems Command (AFSC), United States Air Force, under Contract F49620-82-C-0035 at the request of Sverdrup Technology, Inc. (STI) for the Arnold Engineering Development Center (AEDC), AFSC, Arnold Air Force Station, Tennessee. The results reported were obtained by the principal author during his tenure as a Southeastern Center for Electrical Engineering Education (SCEE) fellow and by personnel of Sverdrup Technology, Inc., operating contractor for propulsion testing at the AEDC, AFSC, under AEDC Project No. D240. The manuscript was submitted for publication on May 20, 1983.

CONTENTS

	<u>Page</u>
1.0 INTRODUCTION	5
2.0 SUPERSONIC PROBE	6
2.1 Characteristics of Probe Flow Field	6
2.2 Shock Detachment	8
2.3 Particle Trajectories	9
3.0 PARTICLE DYNAMICS	9
3.1 Normal Shock Relations	9
3.2 Particle Parameters Behind Shock	10
3.2.1 Particle Mach Number	10
3.2.2 Local Reynolds Number	11
3.2.3 Particle Knudsen Number	12
3.3 Particle Drag Coefficient	13
3.4 Equation of Particle Motion	15
4.0 SIMILITUDE	17
4.1 Scaling Law for Probe Collection Efficiency	17
4.2 Nozzle-Generated Supersonic Flows	19
4.3 Gas Viscosity	20
4.4 Particle Parameters and Stagnation Conditions	22
4.4.1 Stokes Number	23
4.4.2 Knudsen Number	24
4.4.3 Particle Mach Number	26
4.4.4 Local Reynolds Number	26
4.4.5 Particle Reynolds Number	28
4.4.6 Similarity Parameter	28
5.0 PARTICLE BREAKUP	30
5.1 Maximum Particle Drag	30
5.2 Strength of Agglomerates	34
5.2.1 London-Van der Waals Forces	35
5.2.2 Electrostatic Forces	36
5.2.3 Surface Films	37
5.2.4 Maximum Strength	37
5.3 Strength of ZnO Agglomerates	38
5.4 Strength of Liquid Droplets	39
5.5 Criteria for Particle and ZnO Breakup	40
6.0 SUMMARY AND RECOMMENDATIONS	42
REFERENCES	43

ILLUSTRATIONS

<u>Figure</u>	<u>Page</u>
1. Schematic of Particle Probe in Supersonic Stream	6
2. Shock Wave Detachment Distance Data for Body of Revolution with Flat Nose	8
3. Particle Moving Behind Normal Shock Wave	10
4. Particle Drag Coefficient	14
5. Example of Probe Collection Efficiency for Stokesian Particles	18
6. Schematic of Laval Nozzle	19
7. Free-Stream Mass Flow Rate in Probe Cross-Sectional Area	21
8. Dimensionless Function Proportional to Particle Stokes Number	24
9. Dimensionless Function Proportional to Particle Knudsen Number	25
10. Particle Mach Number Behind a Normal Shock Wave	26
11. Dimensionless Function Proportional to Local Particle Reynolds Number Behind a Normal Shock Wave	27
12. Dimensionless Function Proportional to Particle Reynolds Number, Re_p	29
13. Dimensionless Function Proportional to Particle Stopping Distance for Non-Stokesian Particle ($Re_p \gg 1$)	30
14. Dimensionless Function Proportional to Particle Drag Behind Normal Shock	32
15. Normalized Particle Drag, $\gamma = 1.4$	33
16. Normalized Particle Drag, $\gamma = 1.16$	33
17. Schematic of Particle Agglomerate	34
18. Crushing Strength of ZnO Agglomerates	39

TABLES

1. Typical Gas and Particle Properties Across a Probe Shock in Solid Rocket Plume Sampling	7
2. Dimensionless Groups that Determine Particle Trajectories for a Given Gas Flow Field	17
3. Sutherland's Constant	22
4. Typical Values of $d \rho_o / k$	34
5. Maximum Force of Adhesion between Two Smooth Spheres of 1- μ m Diameter	38
NOMENCLATURE	44

1.0 INTRODUCTION

Liquid and/or solid particulates are typically formed in combustion processes by condensation of supersaturated vapors followed by freezing as the particulates cool. The small (usually sub-micron in size) unit particles so formed may coagulate or agglomerate into larger liquid or solid particles. The nature and size distribution of combustion-produced particles is important from a system performance standpoint as well as, many times, from an environmental standpoint. Thus, measurement techniques for particulates are an important issue. In many cases, *in situ* optical methods may be used, but in others, the density of the particulates or their incandescence may preclude direct measurements, and sample extraction methods must be used. Under normal industrial conditions (e.g., smokestacks), representative particle samples can be extracted from the low velocity flows using isokinetic sampling procedures. However, when the particle-laden stream is flowing at high velocity (even supersonic), the flow around the probe becomes quite complex, and the nature of the sample collected is directly related to the complex flow pattern. This is the situation encountered in the exhaust plumes of rocket and turbine engines and in some wind tunnels. In this study, the problems encountered in sampling the exhaust flow from a solid propellant rocket motor being tested at simulated high altitude are examined.

Probe designs which must be immersed in the exhaust plumes of solid propellant rocket motors must withstand the high velocity (≈ 6000 ft/sec), high temperature ($> 3,500^\circ\text{K}$) environment. The systems are further constrained by the physical arrangement and dimensions of the test facilities. Thus, isokinetic sampling can rarely be accomplished, and the effects of the flow on the sample integrity must be assessed. In this case, particle sampling from a supersonic stream will produce a detached shock wave in front of the particle collection probe. The shock front creates a velocity difference between the free stream and the gas entering the sampling probe, and a size-dependent preferential withdrawal of particles may take place. In addition, the large drag forces which result from the particle-shock interaction can cause the breakup of droplets and particle agglomerates.

The purpose of this study is to identify the form of the scaling laws and important dimensionless groups which are expected to play a role in the collection efficiency of a supersonic probe. Important particle parameters which apply to the dynamics of particle motion behind a normal shock wave are identified. These dimensionless groups are related to the stagnation conditions or boundary conditions imposed in most rocket motor-generated supersonic flows. Finally, criteria for agglomeration and droplet or agglomerate breakup are established in terms of the forces of adhesion and particle drag.

2.0 SUPERSONIC PROBE

The simplest probe geometry is a straight-walled cylindrical tube aligned parallel to the free stream as shown in Fig. 1. More complicated probe geometries, such as the type described in Ref. 1, involve the use of a diverging nozzle within the probe inlet. This additional feature is designed to provide isokinetic sampling conditions up to a Mach number of 1.2 with a "shock down" region downstream from the probe inlet. In many applications, however, such as particle sampling in solid rocket motor plumes with stagnation temperatures of $\approx 4,000^\circ\text{K}$ and pressures in the range from 500 to 1,000 psia (Refs. 2 and 3), the gas Mach number at the rocket nozzle exit plane is about 4 or greater, and gas velocities are greater than 3000 m/sec. Furthermore, the solid particulate content may be as large as 30 percent by weight. To withstand such environments, ablative probe designs are used in which the probe frontal area is blunted, negating the possibility of isokinetic sampling. Furthermore, the high Mach numbers make it difficult to design an inlet and internal geometry within the probe which will capture the particles in an isokinetic manner.

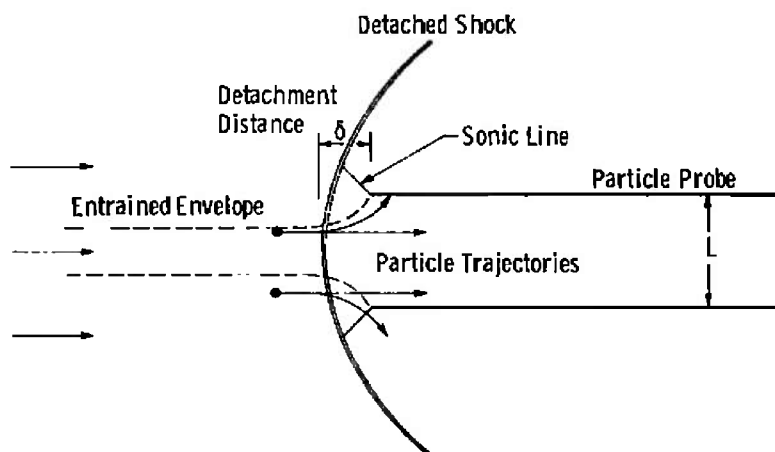


Figure 1. Schematic of particle probe in supersonic stream.

2.1 CHARACTERISTICS OF PROBE FLOW FIELD

The flow field near the inlet of the sampling probe, as shown in Fig. 1, is similar to the flow field which exists in the vicinity of a supersonic pitot tube (Ref. 4). An essential difference, however, is that the particle probe in the present case admits gas into the inlet. The effects of heat transfer and friction will normally choke the flow in the probe in such a way that the initial Mach number at the probe inlet is subsonic (Ref. 5) rising to sonic at the probe outlet. In this case the probe is unable to pass all of the free-stream flow corresponding to its cross-sectional area, and part of the flow will spill over the inlet lip. The

fraction of fluid which spills over will determine the position of the fluid streamlines behind the shock wave near the probe inlet; moreover, the fraction of fluid lost to the mainstream will be independent of the probe exhaust pressure, provided that it is sufficiently low.

The entrained fluid from the free stream is indicated by the envelope shown in Fig. 1. The flow is subsonic in the region bounded by the detached shock, the probe walls, and the sonic line which intersects the probe inlet.

Typical fluid properties across the shock wave along the probe centerline are indicated in Table 1 for sampling near the nozzle exit of a solid rocket plume. Across the shock wave, in this application, the fluid density remains sufficiently low that the mean free path of the gas (λ) is about $0.5 \mu\text{m}$. If the flow is choked, the gas Mach number inside the probe inlet will be less than the value of M_2 indicated in Table 1. The fluid Reynolds number (Re_L) behind the shock wave based on a probe diameter of 2.54 cm is sufficiently large that the boundary layers are very thin and viscous effects on the character of the flow field are relatively unimportant.

Table 1. Typical Gas and Particle Properties Across a Probe Shock in Solid Rocket Plume Sampling

Stagnation Conditions (Ref. 3)	Gas Properties Upstream of Shock	Gas Properties Downstream of Shock	Particle Parameters Downstream of Shock ($d = 1\mu\text{m}$)
$T_0 = 3420^\circ\text{K}$	$M_1 = 4$	$M_2 = 0.35$	$Re_2 = 5.6$
$P_{01} = 590 \text{ psi}$	$V_1 = 3050 \text{ m/sec}$	$V_2 = 402 \text{ m/sec}$	$M_{p2} = 2.3$
$P_{02} = 27.6 \text{ psi}$	$C_1 = 762 \text{ m/sec}$	$C_2 = 1148 \text{ m/sec}$	$Kn \cong 0.5$
$\gamma = 1.16$	$T_1 = 1500^\circ\text{K}$	$T_2 = 3390^\circ\text{K}$	$St^* = 0.83$
	$P_1 = 1.5 \text{ psi}$	$P_2 = 26 \text{ psi}$	$Re_p = 6.44$
	$\rho_1 = 0.21 \times 10^{-4} \text{ gm/cm}^3$	$\rho_2 = 1.6 \times 10^{-4} \text{ gm/cm}^3$	$St^*/Re_p^{2/3} = 0.24$
		$R_L^* = 2.1 \times 10^4$	$Wb^{**} \cong 20-200$

*Probe diameter = 2.54 cm

** $2 \times 10^5 \text{ dynes/cm}^2 < P/A_p < 2 \times 10^6 \text{ dynes/cm}^2$ from Fig. 18

The particle dimensionless parameters for a unit density sphere of diameter $d = 1\mu\text{m}$ are also shown in Table 1. These particle parameters, defined in detail in the text, are as follows:

Reynolds Number = dynamic forces/viscous forces

Mach Number = particle-gas velocity difference/local sonic velocity

Knudsen Number = gas mean free path/particle diameter

Stokes Number = particle stopping distance/characteristic length (probe diameter)

Weber Number = inertial (drag) forces/surface binding forces (adhesion)

2.2 SHOCK DETACHMENT

The shock detachment distance (δ) in Fig. 1 cannot be predicted without extensive numerical calculations. The magnitude of δ , however, is scaled by the diameter of the probe and is dependent on the free-stream Mach number M_1 . Figure 2 illustrates the results of experimental measurements for a flat-nosed, solid body of revolution (Ref. 4). The fluid

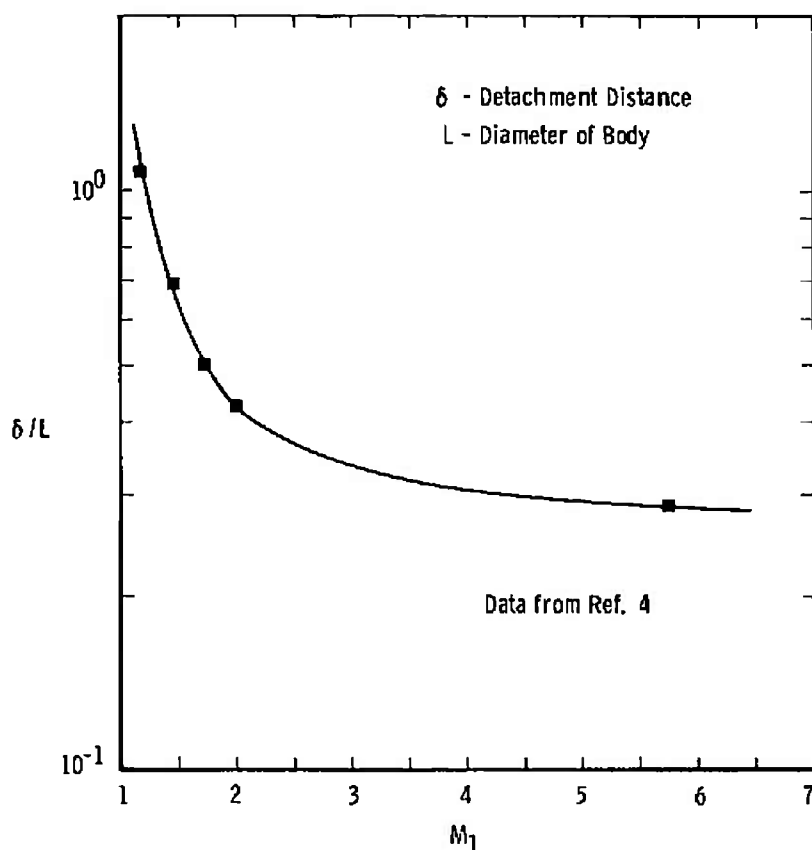


Figure 2. Shock wave detachment distance data for body of revolution with flat nose.

entrained into the probe may reduce the ratio somewhat, but a full numerical solution would be necessary to determine the effect. For the experimental results of Fig. 2, $\delta/L = 0.35$ for $M_1 > 2$ with a maximum of 14 percent error. It is unlikely that the relative position of the gas streamlines will be affected strongly for larger Mach numbers provided the fraction of fluid lost to the mainstream at the probe inlet remains constant.

2.3 PARTICLE TRAJECTORIES

Particles have significant inertia relative to the surrounding fluid since liquid and solid particle densities are much larger than that of the carrier gas. Particles within the entrained envelope upstream of the shock wave in Fig. 1 will either follow the fluid streamlines if they are small, or project across streamlines into the probe inlet if they are large enough. If the volume of gas spilling over the probe lip is large and the probe fluid intake is small, some of the particles initially moving near the inner edge of the entrained envelope will subsequently make contact with the inner walls of the probe lip. The radius of curvature of the fluid streamlines can be very small in this region of the flow field. Particle deposition of a similar type has been observed in both axisymmetric and two-dimensional ambient particle samplers (Refs. 6 and 7). More significantly, large particles outside the entrained envelope will project across fluid streamlines into the probe, increasing the large particle concentration of the sampled gas over that of the free stream. (Ref. 8).

3.0 PARTICLE DYNAMICS

Particles suspended in the supersonic streams of rocket plumes, high-speed wind tunnels, and shock tubes often encounter shock waves. When a particle encounters a shock front, it projects ahead of the carrier gas moving behind the discontinuity because of its inertia and the sharp decrease in gas velocity. This phenomenon subjects the particle to a large drag force behind the shock wave, and the particle motion relaxes eventually to that of the carrier gas.

3.1 NORMAL SHOCK RELATIONS

For simplicity, a perfect gas is assumed with constant specific heats. The relationships between gas properties across a normal shock wave are listed below. Reference will be made to these expressions in the calculations that follow. Referring to Fig. 3,

$$\frac{\rho_1}{\rho_2} = \frac{v_2}{v_1} = \frac{(\gamma - 1) M_1^2 + 2}{(\gamma + 1) M_1^2} \quad (1)$$

$$\frac{T_2}{T_1} = \frac{\left[1 + \left(\frac{\gamma - 1}{2} \right) M_1^2 \right] \left[\left(\frac{2\gamma}{\gamma - 1} \right) M_1^2 - 1 \right]}{\frac{(\gamma + 1)^2 M_1^2}{2(\gamma - 1)}} \quad (2)$$

where M_1 is the Mach number ahead of the shock and γ is the constant ratio of specific heats for the gas.

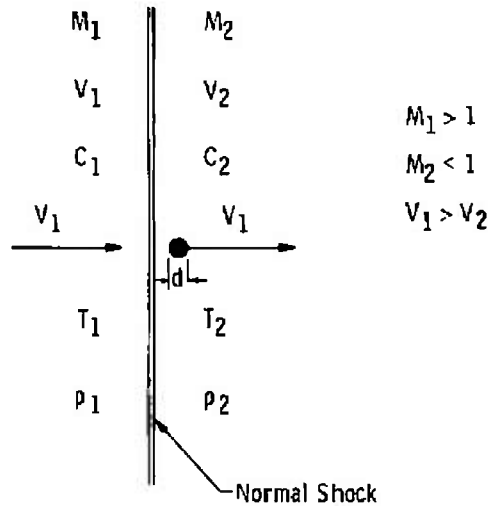


Figure 3. Particle moving behind normal shock wave.

3.2 PARTICLE PARAMETERS BEHIND SHOCK

Three local particle parameters can be defined behind a shock front. The three dimensionless groups are local values of the particle Mach, Reynolds, and Knudsen numbers. As shown below, only two of these groups are independent and required to determine the particle drag coefficient.

3.2.1 Particle Mach Number

The particle Mach number is defined as the speed of the particle relative to the carrier gas divided by the local speed of sound. Particle Mach number is not defined elsewhere in the literature. In particle-shock interactions, the particle Mach number is a maximum directly behind the shock wave and decreases to zero as the particle slows to the speed of the ambient fluid. In general, the particle Mach number can be written as

$$M_p = \frac{|\vec{v} - \vec{v}_f|}{c_2} \quad (3)$$

where \vec{v} and \vec{v}_f are the local particle and gas velocities. Immediately behind the shock wave, returning to Fig. 3 and the expression above, one obtains a maximum value for M_p of

$$M_{p2} = \frac{v_1 - v_2}{c_2} = \left(1 - \frac{v_2}{v_1}\right) \left(\frac{c_1}{c_2}\right) \left(\frac{v_1}{c_1}\right) \quad (3a)$$

Since the local speed of sound is $c = (\gamma RT)^{1/2}$ where R is the specific gas constant and $M_1 = v_1/c_1$, Eq. (3a) becomes

$$M_{p2} = \left(1 - \frac{v_2}{v_1}\right) \left(\frac{T_1}{T_2}\right)^{1/2} M_1 \quad (4)$$

Substituting from Eqs. (1) and (2) above, one has

$$M_{p2} = \frac{\left(\frac{2}{\gamma - 1}\right)^{1/2} (M_1^2 - 1)}{\left[1 + \left(\frac{\gamma - 1}{2}\right) M_1^2\right]^{1/2} \left[\frac{2\gamma}{\gamma - 1} M_1^2 - 1\right]^{1/2}} \quad (5)$$

For weak shocks ($M_1 \approx 1$), Eq. (5) indicates that the particle Mach number behind the shock wave vanishes. As the gas Mach number increases, however, M_p approaches an upper limit. From Eq. (5),

$$\begin{aligned} M_1 \rightarrow 1, \quad M_{p2} \rightarrow 0 \\ M_1 \rightarrow \infty, \quad M_{p2} \rightarrow \left[\frac{2}{\gamma(\gamma - 1)}\right]^{1/2} \end{aligned} \quad (6)$$

In the case of a rocket exhaust for $\gamma \approx 1.16$ (Ref. 3), the upper limit for the magnitude of M_{p2} is $M_{p_{\max}} = 3.28$. For air with $\gamma = 1.4$, $M_{p_{\max}} = 1.89$.

3.2.2 Local Reynolds Number

The local Reynolds number of a particle is defined in terms of the particle diameter and its velocity relative to the ambient fluid. As is the case for the particle Mach number, the particle Reynolds number is a maximum behind the shock front and decreases to zero as the

particle equilibrates with the gas motion. Thus, behind the shock front, one obtains a local Reynolds number in the form

$$Re = \frac{\rho_2 |\vec{v} - \vec{v}_f| d}{\mu_2} \quad (7)$$

Immediately behind the shock, however, the particle Reynolds number becomes

$$Re_{p2} = \frac{\rho_2 (v_1 - v_2)d}{\mu_2} \quad (7a)$$

3.2.3 Particle Knudsen Number

The particle Knudsen number is defined as the ratio of the gas mean free path to the particle diameter, or

$$Kn = \lambda/d \quad (8)$$

where, downstream of a normal shock wave (Ref. 9),

$$\lambda = \frac{\mu_2}{\rho_2} \left(\frac{\pi m}{2k_b T_2} \right)^{1/2} \quad (9)$$

Here, m is the molecular mass and k_b is Boltzmann's constant. Taking the ratio of the local values of the particle Mach and Reynolds numbers as defined by Eqs. (3a) and (7a), one has

$$\frac{M_p}{Re} = \frac{\mu_2}{\rho_2 c_2 d} \quad (10)$$

where the speed of sound is $c_2 = (\gamma R T_2)^{1/2}$. Rearranging Eq. (10) and comparing with Eqs. (8) and (9), one obtains

$$Kn = \left(\frac{\pi}{2} \right)^{1/2} \gamma^{1/2} \frac{M_p}{Re} \quad (11)$$

Thus, only two of the three dimensionless particle groups are independent in the flow field. It should be noted that unlike the particle Mach and Reynolds numbers, the Knudsen number remains constant downstream of the shock wave provided the gas properties do not change appreciably. The assumption of constant gas properties is a reasonable one in most cases.

Substituting the maximum particle Mach number Eq. (6) into Eq. (11) yields the inequality

$$\text{Kn Re} \leq \left(\frac{\pi}{\gamma - 1} \right)^{1/2} \quad (12)$$

In other words, the product of the local particle Knudsen and Reynolds numbers must be less than a constant which depends on the ratio of specific heats of the gas.

3.3 PARTICLE DRAG COEFFICIENT

Newton's law for a spherical particle moving relative to a gas is

$$m_p \frac{d\vec{v}}{dt} = \frac{\rho}{2} A_p C_D |\vec{v} - \vec{v}_f| (\vec{v} - \vec{v}_f) \quad (13)$$

where \vec{v} is the particle velocity, \vec{v}_f is the fluid velocity, m_p is the mass of the particle, ρ is the fluid density, C_D is the drag coefficient, and $A_p (= \pi d^2/4)$ is the cross-sectional area of the particle.

In general, the drag coefficient (C_D) depends on local values of any two of the three groups given by the particle Mach, Reynolds, and Knudsen numbers as discussed in Sec. 3.2.3. Extensive research has been conducted on values of C_D for particles moving at both supersonic and subsonic speeds covering a wide range of particle Knudsen numbers in both the free molecular and continuum regimes (Refs. 10, 11, and 12). A useful expression developed by Crowe (Ref. 11) which correlates drag data in supersonic flows and reduces to Stokes law in the continuum is given below.

$$C_D = (C_D^0 - 2) \exp[-3.07 \gamma^{1/2} M_p \omega(\text{Re})/\text{Re}] \\ + f(M_p)/\gamma^{1/2} M_p \exp(-\text{Re}/2M_p) + 2 \quad (14)$$

where

$$\ln \omega(\text{Re}) = 2.88 [1 + \tanh(0.33 \ln \text{Re} - 1.92)]$$

and

$$f(M_p) = [2.3 + 1.7 (T_p/T_g)^{1/2}] - 2.3 \tanh(0.51 \ln M_p)$$

and (Refs. 8 and 13)

$$C_D^o = \frac{24}{Re} (1 + 0.158 Re^{2/3}) \quad (15)$$

Here, T_p/T_g is the ratio of particle to gas temperature.

Contours of the drag coefficient for constant Knudsen number, from Eq. (14), are plotted in Fig. 4. Values of the drag coefficient for particles crossing a shock follow a contour of constant Kn in Fig. 4 from an initial large particle Re given by Eq. (7) to vanishingly small values when $Re \rightarrow 0$. Also shown in Fig. 4 is the inequality of Eq. (12). Values of the drag coefficient for a given particle must begin above the dashed line to the left of the bifurcation point (located at $Re \approx 28$) or below the dashed line to the right of $Re \approx 28$. In addition, for $Kn \ll 1$, Stokes law (given by $C_D = 24/Re$) and modifications to Stokes law in the inertial regime are indicated.

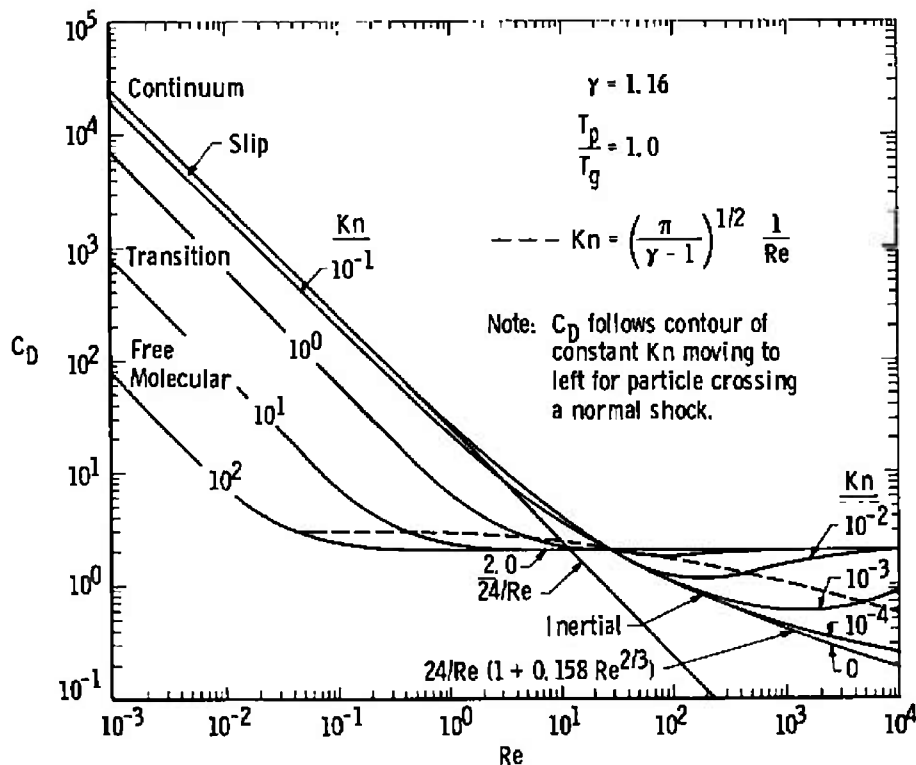


Figure 4. Particle drag coefficient.

Several simple expressions for the drag coefficient can be written in limiting cases, as shown below.

Stokes:

$$C_D = \frac{24}{Re} ; \quad Kn \ll 1, Re < 1 \quad (16)$$

Stokes with slip:

$$C_D = \frac{24}{CRe} ; \quad Kn > 1, Re < 1 \quad (17)$$

where (Ref. 14)

$$C = 1 + 2Kn \left[1.257 + 0.4 \exp\left(-\frac{0.55}{Kn}\right) \right] \quad (18)$$

Non-Stokesian:

$$C_D = \frac{24}{Re} (1 + 0.158 Re^{2/3}) ; \quad Kn \ll 1, Re > 1 \quad (19)$$

3.4 EQUATION OF PARTICLE MOTION

Considering particle motion across a normal shock wave, neglecting the contribution of particle acceleration to the drag, and including an arbitrary fluid velocity, \vec{v}_f , enables Eq. (13) to be written in the form, $-C_D/24 Re(3\pi\mu_2 d)(\vec{v} - \vec{v}_f)$ where Re is the local Reynolds number of the particle and μ_2 is the fluid viscosity behind the shock. Moreover, we assume as before that only small changes in absolute gas temperature occur in the flow field behind the shock wave. The local particle Reynolds number appearing in Eq. (20) as defined by Eq. (7) is conveniently expressed in terms of a reference particle Reynolds number (Re_p) in Eq. (21).

$$m_p \frac{d\vec{v}}{dt} = - \frac{3\pi}{24} C_D Re \mu_2 d (\vec{v} - \vec{v}_f) \quad (20)$$

$$Re = Re_p \frac{|\vec{v} - \vec{v}_f|}{v_1} = Re_p |\vec{v}^+ - \vec{v}_f^+| \quad (21)$$

where

$$Re_p = \frac{\rho_2 d v_1}{\mu_2} \quad (22)$$

and

$$|\vec{v} - \vec{v}_f| = [(\mu - u_f)^2 + (v - v_f)^2 + (\omega - \omega_f)^2]^{1/2}$$

for fluid and particle velocities u , v , and w in three orthogonal directions x , y , and z . Re_p in Eq. (22) is defined in terms of the free-stream gas velocity upstream of the shock, and \vec{v}^+ and \vec{v}_f are the normalized particle and fluid velocities, respectively (Ref. 8).

If Eq. (20) is divided by the particle mass (m_p), the initial particle velocity (v_1), and a characteristic length (L) corresponding to the probe diameter, and if changes in fluid properties behind the shock wave are overlooked, then the nondimensional form of Eq. (20) becomes

$$\frac{d\vec{v}^-}{d\Theta} = -C_D \left(\frac{Re_p}{24} \right) \left(\frac{1}{St} \right) |\vec{v}^+ - \vec{v}_f^+| (\vec{v}^+ - \vec{v}_f^+) \quad (23)$$

subject to the boundary conditions

$$\Theta = 0 : |\vec{v}^+| = 1, |\vec{v}_f^+| = \frac{v_2}{v_1} \quad (24)$$

Here, $\Theta = v_1 t / L$, $C_D = C_D(Re, Kn)$, and St is the particle Stokes number representing the ratio of the particle stopping distance to the characteristic length, or

$$St = \frac{\rho_p d^2 v_1}{18 \mu_2 L} \quad (25)$$

It is also important to note in Eq. (23) that \vec{v}_f^+ is determined by the free-stream Mach number (M_1) and the fraction of fluid geometrically incident on the probe ahead of the shock which subsequently spills over the inlet lip.

Equation (23) has been written to include particle motion in more than one dimension. The particle trajectories determined from Eq. (23), in any case, are defined for a given flow field \vec{v}_f^+ by the dimensionless particle groups Re_p , St , and Kn given by Eqs. (11), (22), and (25).

It is now instructive to look at simple approximations to the dimensionless quantity $C_D Re_p / St$ appearing in Eq. (23). Introducing Eqs. (16) through (19) for C_D , one is able to construct Table 2, listing the important groups which determine the particle trajectories from a given gas flow field.

Table 2. Dimensionless Groups that Determine Particle Trajectories for a Given Gas Flow Field

<u>Group</u>	<u>Limitations</u>
St^*	$Kn \ll 1, Re_p < 1$
$C St^{**}$	$Kn \geq 1, Re_p < 1$
St, Re_p	$Kn \ll 1, Re_p > 1$
$St/Re_p^{2/3}$	$Kn \ll 1, Re_p \gg 1$

*Increase in Stokes number indicates particles with greater inertia.

$$^{**}C = 1 + 2Kn [1.257 + 0.4 \exp(-0.55/Kn)]$$

4.0 SIMILITUDE

It is necessary to understand the form of the scaling law in the collection of particles with a supersonic probe for the purpose of laboratory testing and interpreting experimental data. The collection efficiency will depend, in general, on the properties of the gas flow field and the trajectories of the particles.

4.1 SCALING LAW FOR PROBE COLLECTION EFFICIENCY

Considerable work has been conducted on the problem of isokinetic sampling in subsonic incompressible flows (Ref. 15). Very little research has been conducted on probe characteristics in compressible flows. Dimensional arguments suggest that the probe collection efficiency represented by the ratio of particle concentration (defined as particles per unit mass of carrier gas for compressible flows) to that in the mainstream must be a function of the gas sample rate in the probe in addition to groups characterizing the gas flow field and particle motion. Assuming that viscous effects are negligible in the gas, one obtains an expression for particle collection efficiency of the form

$$\frac{n_s}{n_m} = f\left(\frac{q_m}{q_s}, M_1, St, Kn, Re_p\right) \quad (26)$$

where n_s is the number of particles per unit mass in the probe sample line, n_m is the number of particles per unit mass in the mainstream upwind of the detached shock, q_m is the mass flow rate of gas in the mainstream in the probe cross-sectional area A , and q_s is the mass flow rate of gas in the probe sample line.

For gas Mach numbers $M_1 > 2$, the dimensions of the flow field back of the shock wave near the probe inlet remain relatively constant, as indicated in Fig. 2. If the particles are limited by one of the conditions of Table 2 (e.g., Stokesian with $Re_p < 1$), the probe collection efficiency reduces to

$$\frac{n_s}{n_m} = f\left(\frac{q_m}{q_s}, St, M_1\right) \quad (27)$$

where M_1 may be of secondary importance. An example of the form of the collection efficiency is shown in Fig. 5. It should be noted in Fig. 5 that small particles ($St \ll 1$) follow the fluid streamlines and $n_s/n_m \rightarrow 1$. Large particles ($St \gg 1$), however, project straight into the probe inlet when conservation of particle mass suggests $n_s q_s = n_m q_m$. These limits are indicated in Fig. 5.

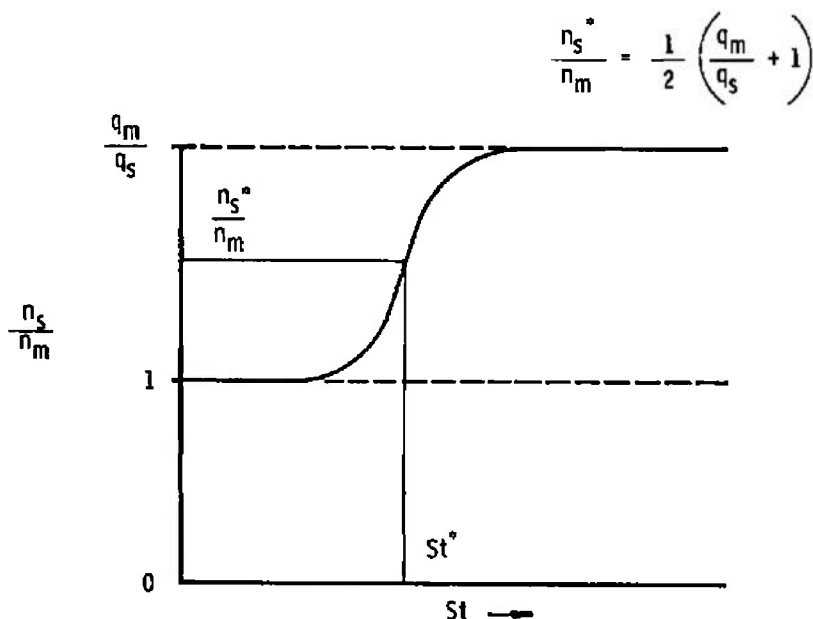


Figure 5. Example of probe collection efficiency for Stokesian particles.

The shape of the efficiency curve, as shown in Fig. 5, will be sigmoidal, which is typical of the performance characteristics of aerosol samplers (Ref. 16). Moreover, St^* , indicated in Fig. 5, corresponds to the critical Stokes parameter for which the collection efficiency is intermediate between its maximum and minimum values. For particle projection into a void, $St^* \approx 0(1)$. Values of St^* are useful for a given flow field, since one can determine the critical particle diameter from its definition given by Eq. (25). Particles smaller than d^* follow the flow field, while larger particles project into the probe from outside the entrained envelope.

In Eqs. (26) and (27), q_s is the mass flow rate in the sample line which depends on friction losses (i.e., friction factor and probe length), heat transfer from the line, and gas Mach number (M_1). The quantity q_s is difficult to predict but can be measured experimentally. The mass flow rate of the free stream (g_m), however, can be determined from gas properties in many important types of supersonic flows as shown in Section 4.2. These considerations lead directly to the design of experiments to measure the particle collection efficiency of different probe geometries.

4.2 NOZZLE-GENERATED SUPERSONIC FLOWS

The basic aerodynamic element used to obtain prescribed supersonic flows is the converging-diverging channel of the type shown in Fig. 6. The nozzle is supplied with gas at a high pressure (the stagnation pressure) at the inlet where the gas velocity is small. Along with pressure, a stagnation temperature of the gas is also prescribed. Provided the exhaust pressure is sufficiently low, sonic conditions exist in the nozzle throat, and the gas Mach number at any position along the axis of the nozzle for a given ratio of specific heats is determined by the ratio of the local cross-sectional area to that of the throat. The same basic configuration exists in the nozzle of a solid fuel rocket motor.

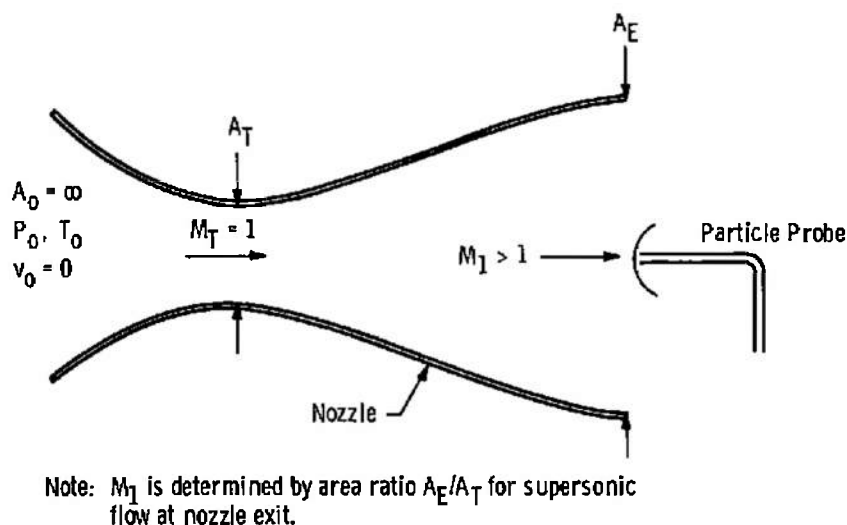


Figure 6. Schematic of Laval nozzle.

The nozzle shown in Fig. 6 is a useful tool for the testing of probes to be used in supersonic flow. The prescribed boundary conditions in these tests are the stagnation conditions of the gas and the nozzle geometry. Prediction of particle parameters can be made in terms of these boundary conditions as demonstrated in Section 4.4. These results are useful in the scaling of probe experiments and for the comparison of probe performance with field tests (e.g., rocket testing).

If the nozzle shown in Fig. 6 is designed to function without significant separation along the inside walls, the flow is approximately isentropic, and gas properties immediately upstream of a shock are related to stagnation conditions by the following expressions:

$$\frac{T_o}{T_1} = 1 + \left(\frac{\gamma - 1}{2} \right) M_1^2 \quad (28)$$

and

$$\frac{\rho_o}{\rho_1} = \left[1 + \left(\frac{\gamma - 1}{2} \right) M_1^2 \right]^{-\frac{1}{\gamma - 1}} \quad (29)$$

The quantity q_m , the mass flow rate in the free-stream incident on the probe area A , can be determined with Eqs. (28) and (29). Since

$$q_m = P_1 v_1 A = \left(\frac{\rho_1}{\rho_o} \right) \left(\frac{v_1}{c_1} \right) \left(\frac{c_1}{c_o} \right) \rho_o c_o A \quad (30)$$

one has

$$\frac{q_m}{\rho_o A \sqrt{R T_o}} = \left(\frac{P_1}{P_o} \right) M_1 \left(\frac{T_1}{T_o} \right)^{1/2} \quad (31)$$

Substituting from Eqs. 28 and 29, one obtains

$$\frac{q_m}{\rho_o A \sqrt{R T_o}} = \frac{\gamma^{1/2} M_1}{\left[1 + \left(\frac{\gamma - 1}{2} \right) M_1^2 \right]^{\frac{\gamma - 1}{2(\gamma - 1)}}} \quad (32)$$

This expression is plotted in Fig. 7.

4.3 GAS VISCOSITY

All of the particle parameters discussed in Section 3, with the exception of the particle Mach number (M_p), involve the gas viscosity. The gas viscosity depends strongly on temperature and is a weak function of pressure at very low temperatures. The Sutherland formula (Ref. 9) gives accurate results for common gases such as nitrogen and oxygen,

$$\frac{\mu}{\mu_n} = \left(\frac{T}{T_r} \right)^{3/2} \left[\frac{T_r - T_\theta}{T + T_\theta} \right] \quad (33)$$

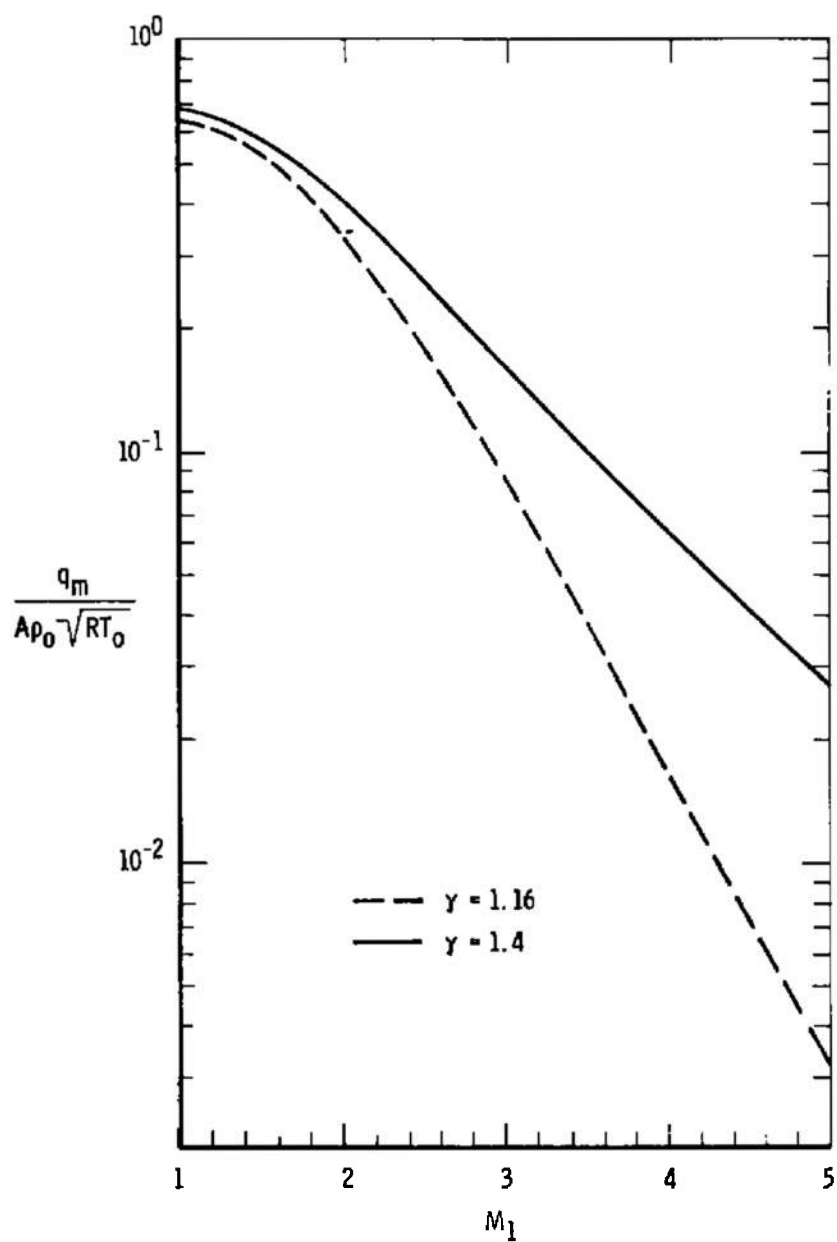


Figure 7. Free-stream mass flow rate in probe cross-sectional area.

where T_r is a reference temperature ($T_r = 298.2^\circ\text{K}$). The quantity $\mu_r = \mu_r(T_r)$ is the viscosity of the gas at the reference temperature and T_θ is Sutherland's constant. Values of T_θ determined empirically for a number of common gases are shown in Table 3, below.

Table 3. Sutherland's Constant*

Gas	T_θ ($^\circ\text{K}$)
Air	111.3
CO_2	239.7
CO	100.0
He	80.3
H_2	72.2
N_2	110.6
O_2	127.0

*From Ref. 17

For simplicity, Eq. (33) can be rewritten in the form

$$\mu = \frac{b T^{3/2}}{T + T_\theta} \quad (34)$$

where

$$b = \mu_r T_r^{1/2} \left(1 + \frac{T_\theta}{T_r} \right) \quad (35)$$

In the case of air, for example, substituting $T_r = 298.2^\circ\text{K}$, $\mu_r = 1.8 \times 10^{-4} \text{ gm/cm-sec}$ and $T_\theta = 111.3^\circ\text{K}$, one obtains a typical value for $b = 1.43 \times 10^{-5} \text{ gm/cm-sec-(}^\circ\text{K)}^{1/2}$. These results will be used in the sections below.

4.4 PARTICLE PARAMETERS AND STAGNATION CONDITIONS

The particle parameters which appear in the equation of motion, Eq. (23), depend on gas properties behind a normal shock wave. The gas properties are related to the gas stagnation conditions, while the Mach number (M_1) upstream of the shock is related to the nozzle design. Thus, expressions can be developed for the important particle parameters in terms of the boundary conditions imposed in the nozzle flow.

4.4.1 Stokes Number

The particle Stokes number is defined as the ratio of the particle stopping distance to a characteristic length in the flow field. Multiplying and dividing by values of the gas properties across the shock wave and in the stagnation region, one finds that Eq. (25) becomes

$$St = \frac{\rho_p d^2 v_1}{18\mu_2 L} = \frac{\rho_p d^2}{18L} \left(\frac{c_o}{\mu_o} \right) \left[\left(\frac{\mu_1}{\mu_2} \right) \left(\frac{\mu_o}{\mu_1} \right) \left(\frac{v_1}{c_1} \right) \left(\frac{c_1}{c_o} \right) \right] \quad (36)$$

Introducing the definition of viscosity from Eq. (34) and noting that $v_1/c_1 = M_1$ and $c_1/c_o = (T_1/T_o)^{1/2}$, we can now write Eq. (36) in the form,

$$St = \left(\frac{\gamma^{1/2}}{k} \right) \left(\frac{\rho_p d^2}{18L} \right) f_1(M_1) \quad (37)$$

where

$$k = b/R^{1/2}$$

and

$$f_1(M_1) = M_1 \left(\frac{T_1}{T_2} \right)^{3/2} \left[\left(\frac{T_2}{T_1} \right) + \left(\frac{T_o}{T_1} \right) \left(\frac{T_o}{T_o} \right) \right] \quad (38)$$

It is interesting to note that Eq. (37) is the product of the particle Stokes number based on the speed of sound of the gas at standard conditions (i.e., a particle moving at Mach 1 at $T = 298.2^\circ K$) and the dimensionless function $f_1(M_1)$. Note also that $f_1(M_1) \approx 1$ as $M_1 \rightarrow 1$.

Numerical solutions of Eq. (38) were determined by introducing Eqs. (1), (2), and (28). Contours of $f_1(M_1)$ are shown in Fig. 8 for a ratio of specific heats $\gamma = 1.4$ for air and $\gamma = 1.16$, typical of solid rocket exhausts. The results shown in Fig. 8 indicate that for constant particle and gas stagnation properties, the particle Stokes number increases with gas Mach number M_1 . This is the result of an increase in the relative velocity between the particle and the gas with Mach number.

Comparing contours of T_o from 300 to 3500°K for $\gamma = 1.4$ in Fig. 8, one concludes that an increase in stagnation temperature (roughly the gas temperature back of the shock) increases the gas viscosity and thus reduces the magnitude of the particle Stokes number.

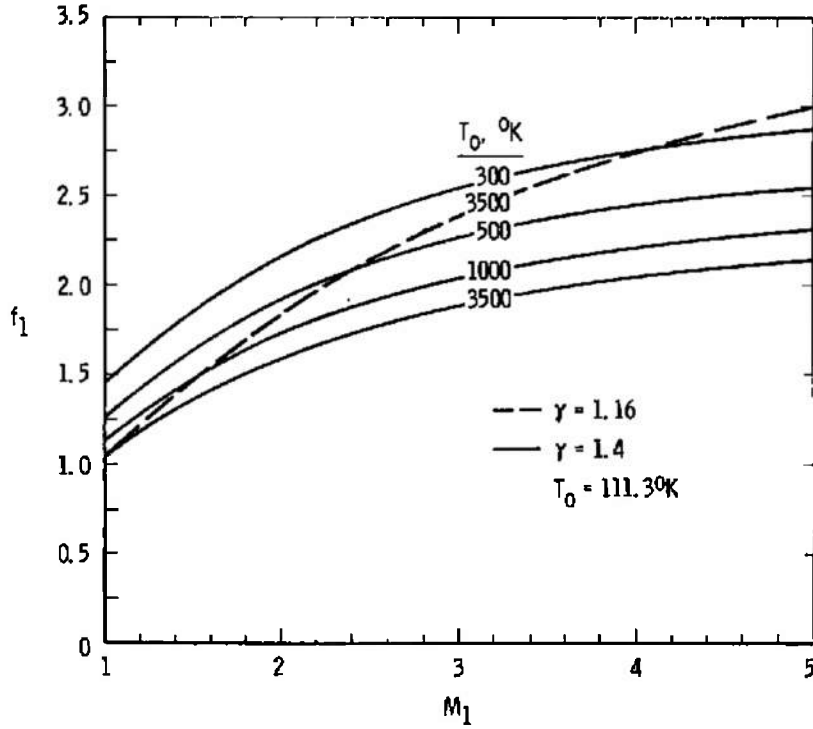


Figure 8. Dimensionless function proportional to particle Stokes number.

4.4.2 Knudsen Number

The particle Knudsen number is defined as the ratio of the mean free path of the gas to the particle diameter. From Eqs. (10) and (11) one has

$$Kn = \left(\frac{\pi}{2}\right)^{1/2} \gamma^{1/2} \frac{\mu_2}{c_2 \varrho_2 d} \quad (39)$$

After some rearrangement using the procedure of the previous section, one obtains an expression in terms of gas stagnation properties, as follows:

$$Kn = \left(\frac{\pi}{2}\right)^{1/2} \left(\frac{k}{dP_o}\right) f_2(M_1) \quad (40)$$

where

$$f_2 = \frac{(T_2/T_1)}{[(T_2/T_1) + (T_o/T_1)(T_\theta/T_o)]} \left(\frac{P_1}{P_2}\right) \left(\frac{P_o}{P_1}\right) \quad (41)$$

Equation (40) is the product of the Knudsen number of the particle in the stagnation region and a dimensionless function, $f_2(M_1)$.

Substituting expressions for the ratios of gas properties appearing in Eq. (41) from Eqs. (1), (2), (28), and (29), one obtains numerical solutions for $f_2(M_1)$, and these results are shown in Fig. 9. As indicated in Fig. 9, $f_2(M_1)$ reaches a minimum for small gas Mach numbers M_1 with

$$f_2(1) \approx \left(\frac{1 + \gamma}{2} \right)^{\frac{1}{\gamma-1}}$$

For constant stagnation conditions, the influence of gas temperature and density appears to cause a decrease in the Knudsen number behind the shock at small M_1 . For larger Mach numbers M_1 , the gas density ρ_2 decreases rapidly, accounting for the increase in Kn.

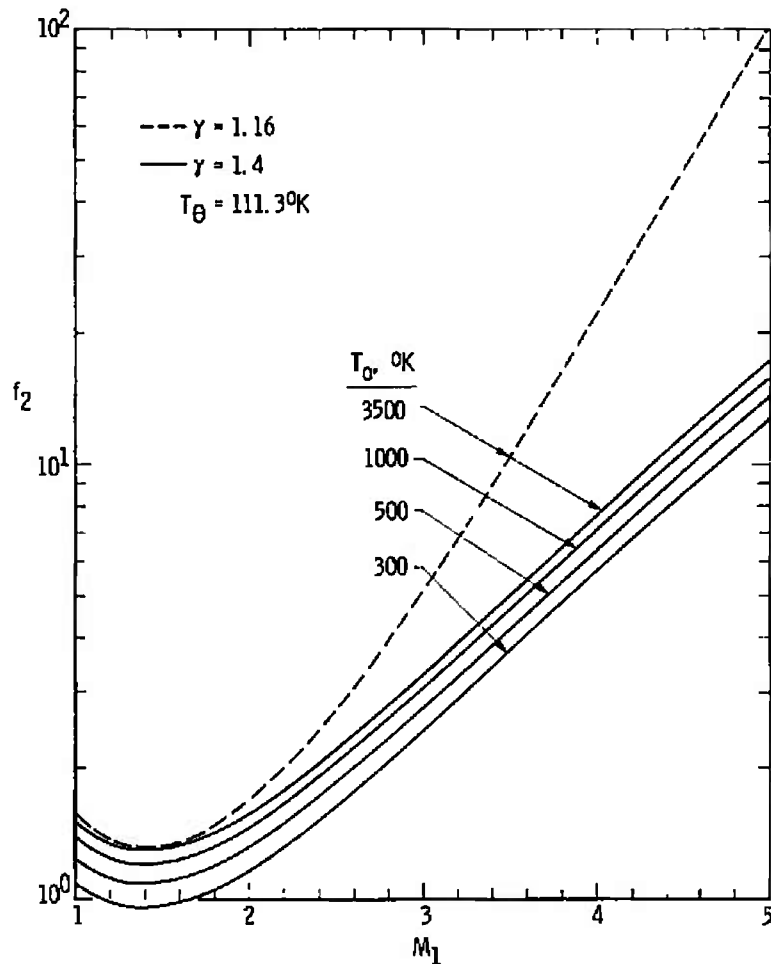


Figure 9. Dimensionless function proportional to particle Knudsen number.

4.4.3 Particle Mach Number

The particle Mach number is the ratio of the velocity of the particle relative to the ambient fluid to the local speed of sound. This particle parameter is summarized in Section 3.2.1. Equation (5) is written as

$$M_{p2} = f_3(M_1) \quad (42)$$

and numerical solutions for this expression are shown in Fig. 10 where $f_3(1) = 0$.

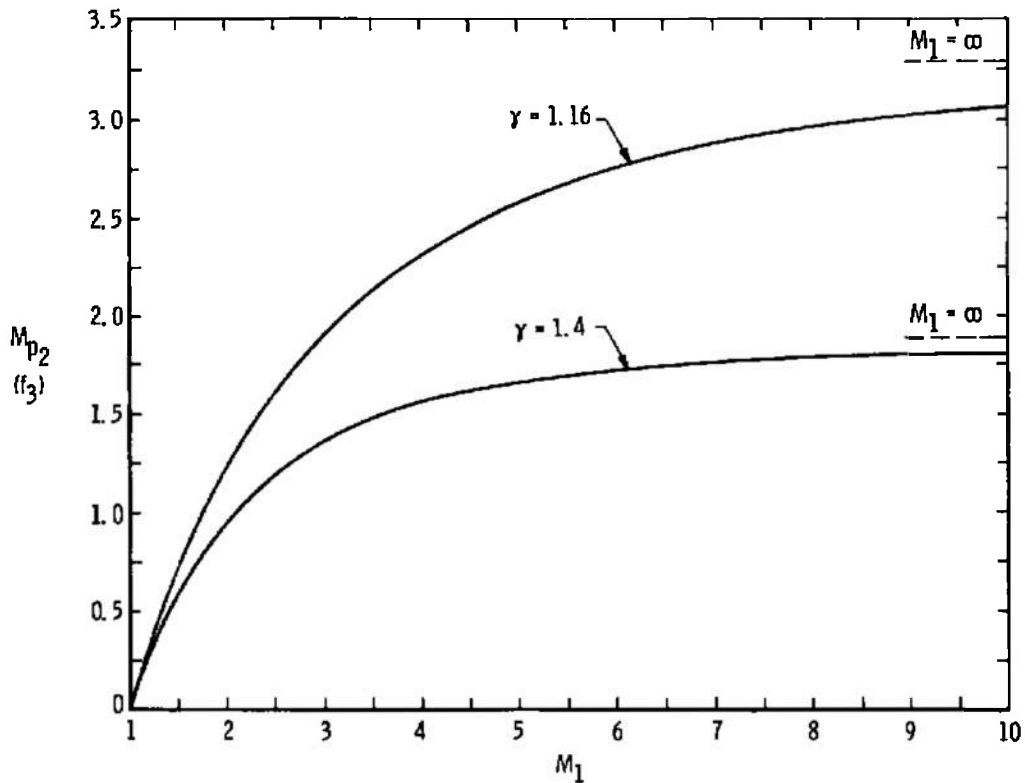


Figure 10. Particle Mach number behind a normal shock wave.

4.4.4 Local Reynolds Number

The local particle Reynolds number represents the ratio of inertial to viscous forces acting on the particle as it moves relative to the gas. From Eqs. (7) and (11), one has a maximum value of

$$Re_2 = \frac{\rho_2}{\mu_2} (v_1 - v_2)d = \left(\frac{\pi\gamma}{2} \right)^{1/2} \frac{M_{p2}}{Kn}$$

where Kn and M_{p2} are defined above in Sections 4.4.2 and 4.4.3 by Eqs. (40) and (42). Thus, one obtains, in terms of stagnation conditions,

$$Re_2 = \gamma^{1/2} \left(\frac{d_{p0}}{k} \right) f_4(M_1) \quad (43a)$$

where

$$f_4(M_1) = f_3(M_1)/f_2(M_1)$$

Numerical solutions to Eq. (43a) in Fig. 11 indicate that the local particle Reynolds number reaches a peak at $M_1 \approx 2$. At smaller values of M_1 (< 2), the relative velocity of the particle with respect to the gas behind the shock wave decreases rapidly and $f_4(1) = 0$. At larger values of M_1 (> 2), the gas viscosity increases. As expected, the group proportional to

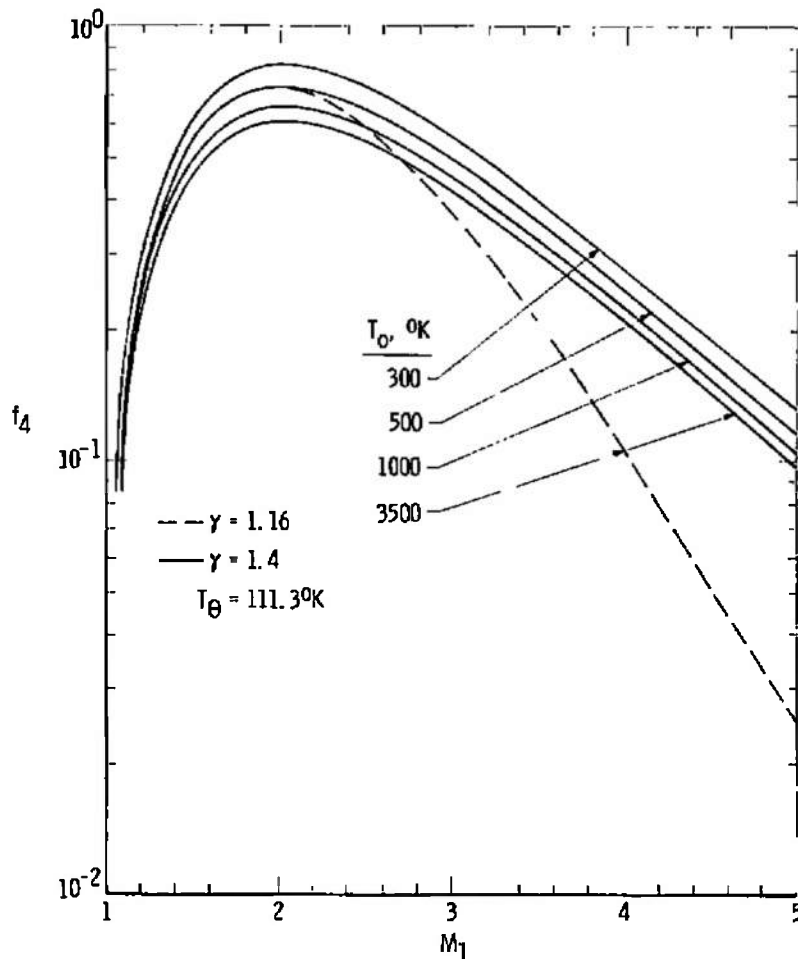


Figure 11. Dimensionless function proportional to local particle Reynolds number behind a normal shock wave.

the particle Knudsen number based on gas properties in the stagnation region, d_{p0}/k , appears in Eq. (43a) as it does in Eq. (40).

4.4.5 Particle Reynolds Number

A particle Reynolds number (Re_p) based on particle velocity ahead of the shock front and on gas properties behind the shock, and defined by Eq. (22), appears in the normalized equation of particle motion, Eq. (23). The magnitude of Re_p determines whether the particle motion can be approximated as Stokesian or non-Stokesian and thus determines the approximate form of the drag coefficient back of the shock front as indicated in Table 2.

From Eqs. (22) and (43) one obtains

$$Re_p = Re_2 \left(1 - \frac{v_2}{v_1} \right) \quad (44)$$

or

$$Re_p = \gamma^{1/2} \left(\frac{d_{p0}}{k} \right) f_5(M_1) \quad (44a)$$

where

$$f_5(M_1) = \frac{f_3(M_1)}{f_2(M_1) \left(1 - \frac{v_2}{v_1} \right)} \quad (44b)$$

Numerical solutions to Eq. (44b) are shown in Fig. 12. Similar to previous calculations for the local particle Reynolds number shown in Fig. 11, contours of $f_5(M_1)$ for constant stagnation temperature peak at $M_1 \approx 2$. It can also be shown that $f_5(1)$ is approximately equal to $[(1 + \gamma)/2]^{1/(1-\gamma)}$.

4.4.6 Similarity Parameter

When the particle Reynolds number defined by Eqs. (22) and (44a) is much greater than one (i.e., $Re_p \geq 10^2$), substitution of the inertial drag coefficient, C_D , from Eq. (19) into the normalized expression for particle motion, Eq. (23), yields the similarity parameter, $St/Re_p^{2/3}$. Physically, this group (like the Stokes number) represents the ratio of the particle stopping distance to the probe diameter. Particle trajectories near the probe inlet will be scaled by this group provided Re_p is large.

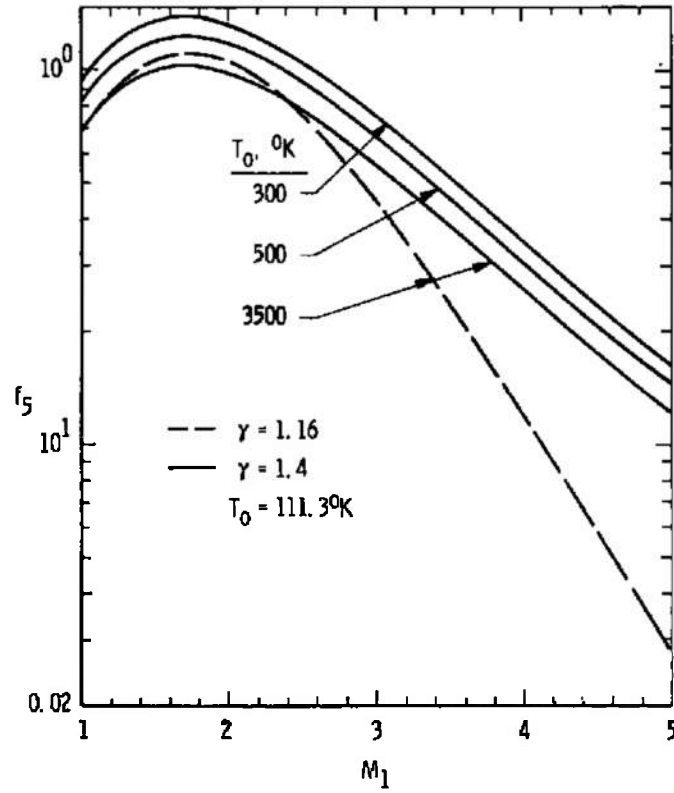


Figure 12. Dimensionless function proportional to particle Reynolds number, Re_p .

Combining Eqs. (22) and (37), one obtains

$$\frac{St}{Re_p^{2/3}} = \frac{\gamma^{1/6}}{k} \left(\frac{e_p d^2}{18L} \right) \left(\frac{k}{d_{Q0}} \right)^{2/3} f_6(M_1) \quad (45)$$

where

$$f_6(M_1) = f_1(M_1) \left(\frac{T_2}{T_1} \right)^{1/3} \left[\frac{f_2(M_1)}{M_1} \right]^{2/3}$$

Numerical solutions to $f_6(M_1)$ show an increase with M_1 for $M_1 > 1.4$ and a large dependence on the ratio of specific heats as shown in Fig. 13. Moreover,

$$f_6(1) \approx \left(\frac{1 + \gamma}{2} \right)^{\frac{2}{3(\gamma-1)}}$$

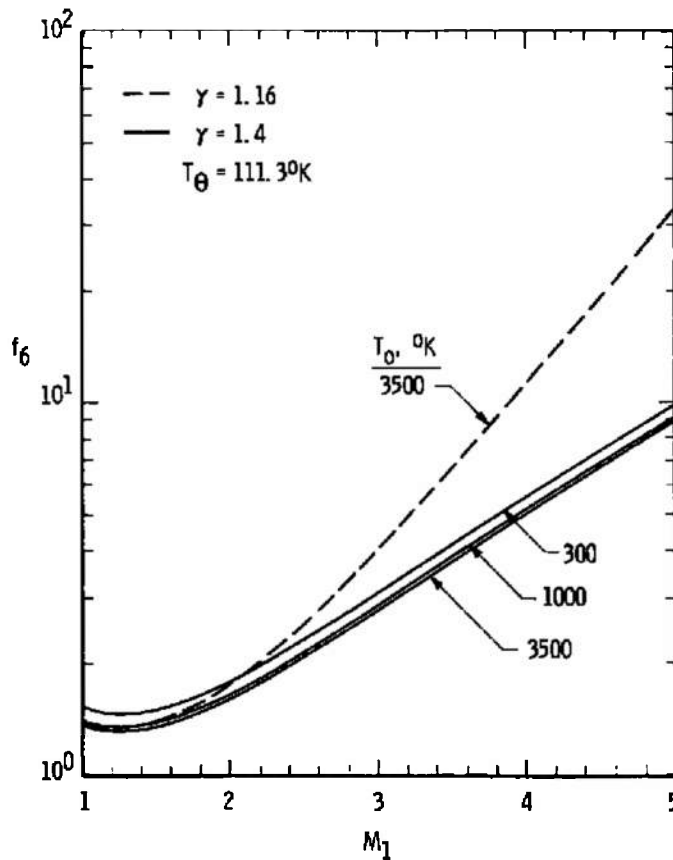


Figure 13. Dimensionless function proportional to particle stopping distance for non-Stokesian particle ($Re_p \gg 1$)

5.0 PARTICLE BREAKUP

Particle agglomerates and liquid droplets are subjected to large shear stresses when they encounter shock waves. The drag forces are greatest in magnitude at the instant the particle passes behind the shock. These forces decrease in magnitude as the particle equilibrates with the gas downstream from the shock. The problem of whether agglomerates and droplets can withstand these stresses without breaking up naturally arises in many types of particle shock interactions.

5.1 MAXIMUM PARTICLE DRAG

The drag on a particle is given by Eq. (13). At the shock, the maximum drag is

$$D = \frac{1}{2} \rho_2 A_p C_D (v_1 - v_2)^2 \quad (46)$$

We now consider nozzle-generated shocks as done in Section 4. If we relate gas properties across the shock and into the stagnation region, Eq. (46) becomes

$$D = \frac{1}{2} C_D A_p \rho_o C_b^2 M_1^2 \left(\frac{T_1}{T_2} \right) \left(\frac{p_2}{p_1} \right) \left(\frac{p_1}{p_o} \right) \left(1 - \frac{v_2}{v_1} \right)^2 \quad (47)$$

Substituting Eqs. (1), (28), and (29) and noting that $\rho_o C_b^2 = P_o$, one obtains

$$\frac{D}{A_p P_o} = C_D \left[\frac{\gamma}{\gamma + 1} \frac{(M_1^2 - 1)^2}{\left[1 + \left(\frac{\gamma - 1}{2} \right) M_1^2 \right]^{\frac{2\gamma - 1}{\gamma - 1}}} \right] \quad (48)$$

or

$$\frac{d}{d M_1} = C_D g(M_1) \quad (49)$$

Since $g \rightarrow 0$ for $M_1 \rightarrow 0$ and ∞ , we set

$$\frac{d g(M_1)}{d M_1} = 0 \quad (50)$$

Solving for M_1 from Eq. (50), one obtains for the position of the maximum in $g(M_1)$,

$$M_1 = (3 + 2\gamma)^{1/2} \quad (51)$$

Substituting Eq. (51) into $g(M_1)$, we find that the maximum in the dimensionless function is

$$g(\max) = \frac{4\gamma(\gamma - 1)}{\left[1 + \left(\frac{\gamma - 1}{2} \right) (3 + 2\gamma) \right]^{\frac{2\gamma - 1}{\gamma - 1}}} \quad (52)$$

Thus if $\gamma = 1.4$, then $g_{\max} = 0.42$ at $M_1 = 2.4$. Contours of $g(M_1)$ illustrating these features are shown in Figs. 14 and 15.

Numerical solutions are now sought for the normalized drag, Eq. (40), with constant gas stagnation conditions and particle properties. Since the drag coefficient is of the form

$$C_D = C_D(Kn, Re_2) \quad (53)$$

where the arguments appearing in Eq. (53) are given by Eqs. (40) and (43a), values of the normalized drag were determined as a function of the gas Mach number M_1 and the

parameter d_{Q_0}/k . These results are shown in Fig. 14 for air ($\gamma = 1.4$) and in Fig. 15 for a gas mixture ($\gamma = 1.16$) typical of solid rocket exhausts.

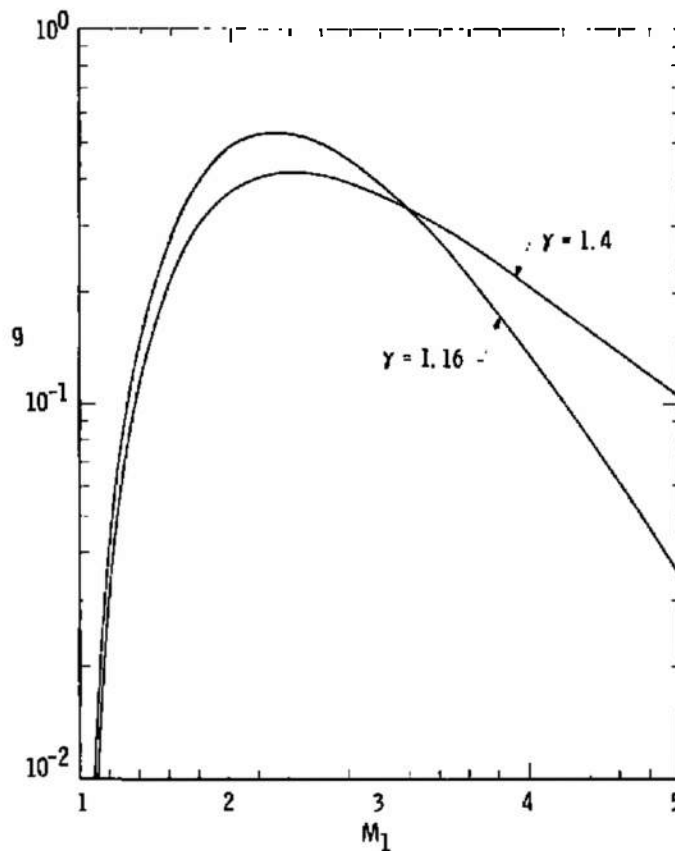


Figure 14. Dimensionless function proportional to particle drag behind normal shock.

The results presented in Figs. 15 and 16 demonstrate that particles will experience the largest stresses at a gas Mach number in the range $2 < M_1 < 2.5$. These results are insensitive to the stagnation temperature, indicating a variation of less than 5 percent for stagnation temperatures in the range $500\text{K} < T_0 < 3500\text{K}$. The results are also insensitive to changes in T_0 , Sutherland's constant, for the values shown in Table 3 as was the case in Figs. 8 through 13.

Expected values of the parameter d_{Q_0}/k proportional to the inverse of the particle Knudsen number in the stagnation region are indicated in Table 4.

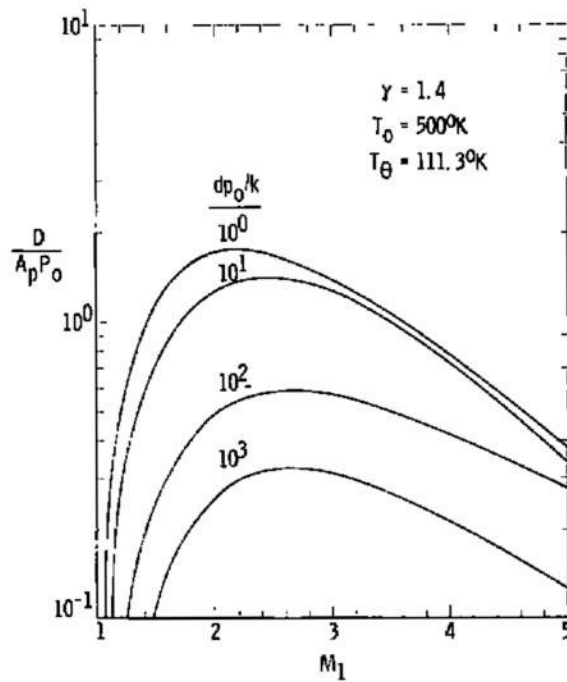


Figure 15. Normalized particle drag, $\gamma = 1.4$.

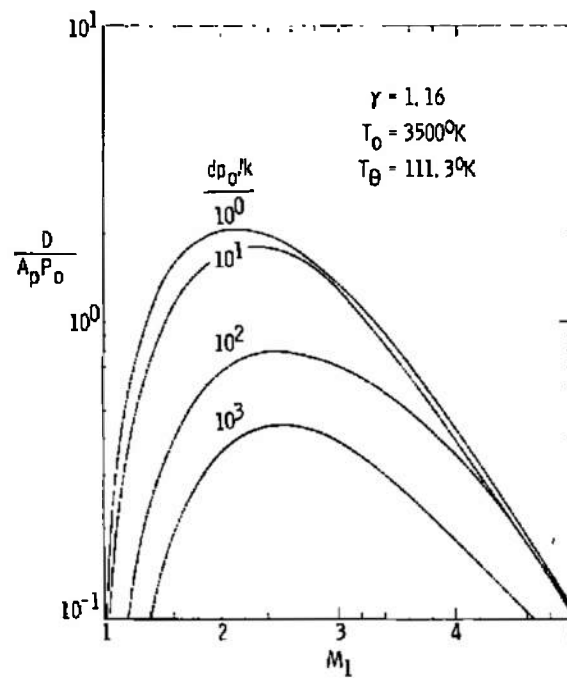


Figure 16. Normalized particle drag, $\gamma = 1.16$.

Table 4. Typical Values of d_{g_0}/k

$d(\mu m)$	$\gamma = 1.16$ $P_o = 600 \text{ psi}$ $T_o = 3500^\circ K$	$\gamma = 1.4$ $P_o = 50 \text{ psi}$ $T_o = 500^\circ K$
	d_{g_0}/k	d_{g_0}/k
1	50	28
10	500	280

$$^*R = 2.86 \times 10^6 \text{ cm}^2\text{-sec}^{-2}\text{-}^\circ K^{-1}$$

$$b = 1.43 \times 10^{-5} \text{ gm-cm}^{-1}\text{-sec}^{-1}\text{-(}^\circ K\text{)}^{-1/2}$$

$$k = .846 \times 10^{-8} \text{ gm-cm}^{-2}$$

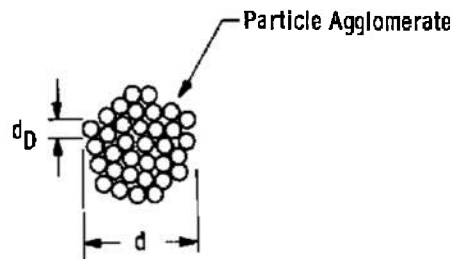
5.2 STRENGTH OF AGGLOMERATES

In the following treatment, we assume that large agglomerates consist of small constituent particles that are uniform spheres of size d_D . An example of an agglomerate is shown in Fig. 17. Following the treatment of Rumpf (Ref. 18), we also assume that the force of adhesion between two constituent particles is F and that each small sphere of size d_D has z contacts (coordination number). If the voidage is $1 - \phi$, the number of spheres per unit cross-sectional area of the large agglomerate is

$$n = \frac{\phi}{\frac{\pi}{4} d_D^2} \quad (54)$$

Thus, the number of contacts per unit cross-sectional area becomes

$$\frac{nz}{2} = \frac{2\phi z}{\pi d_D^2} \quad (55)$$

**Figure 17. Schematic of particle agglomerate.**

where the factor of one-half is introduced in Eq. (55) since each contact is shared by two spheres.

One can now write the total force of p adhesion per unit cross-sectional area of the agglomerate as

$$\frac{P}{A_p} = \frac{\phi z F}{\pi d_D^2} \quad (56)$$

where $A_p = \pi d^2/4$ is the cross-sectional area of the agglomerate, P is the total force of adhesion, and F is the particle bonding force function. In Eq. (56) an additional factor of 1/2 has been introduced by Rumpf (Ref. 18) since each constituent particle must break only half of its contacts to form a cleavage plane. Rumpf also demonstrates that $z(1 - \phi) \approx 3.1$ for common coordination numbers so that Eq. (56) simplifies to

$$\frac{P}{A_p} \approx \frac{\phi}{1 - \phi} \frac{F}{d_D^2} \quad (57)$$

It now remains to examine the various forms that F may take.

5.2.1 London-Van der Waals Forces

The force of adhesion between clean, dry, uncharged particles and surfaces is due to London-Van der Waals type attractive forces. Nonpolar, electrically neutral atoms and molecules have momentary dipoles over short periods of time due to the movement of orbital electrons. Integrating the attractive forces between all of the molecules in two small spheres separated by a distance "a" gives an attractive force of the form

$$F_{v1} = \frac{B_1 d_D}{a^2} \quad (58)$$

The distance in the denominator of Eq. (58) is restricted to $a < 2000\text{\AA}$, and B_1 is typically in the range $10^{-13} < B_1 < 10^{-11}$ ergs (Ref. 14), depending on the nature of the material and the media separating the spheres.

For larger separations, $a > 2000\text{\AA}$, Lifschitz' Eqs. (18), (14), and (19) between two spherical particles of equal diameter are

$$F_{v2} = \frac{B_2 d_D}{a^3} \quad (59)$$

where $B_2 \approx 10^{-20}$ erg-cm and depends on particle composition and the media separating the spheres.

It should be noted that the extensive literature available on the subject of Van der Waals forces demonstrates that the calculations suggested above are only approximate, at best, as reviewed by Davies (Ref. 14). Electrostatic charge and adsorbed liquid on particle surfaces can result in considerable error in the simple calculations above.

5.2.2 Electrostatic Forces

Suspended particles carry electrostatic charge. There are many mechanisms of charging, and these are reviewed by Davies (Ref. 14) and Friedlander (Ref 8). The important mechanisms fall into one of two categories. The particles are charged during their formation or are exposed to electrons and ions carried by the ambient gas. Assuming two spheres with a surface charge density q , separated by a distance " a " much smaller than the diameter of the spheres d_D , the force of attraction is

$$F_e = \frac{\epsilon \pi^2 d_D^2 q^2}{a^2} \quad (60)$$

where $\epsilon = 9 \times 10^{18}$ dynes-cm²/coul is Coulomb's law constant.

In the case of particle charging, one encounters a charge limit (Ref. 14). This represents the maximum electrical charge that can be carried by the particle before spontaneous emission of electrons or ions occurs. For a spherical particle, the limiting electron or ion charge is given by the expression

$$n_p = K_p d_D^2 \quad (61)$$

where n_p represents the number of coulombs of charge and $K_p = 2.72 \times 10^{-6}$ coul/cm² or $K_p = 5.44 \times 10^{-5}$ coul/cm² for the electron and ion limit, respectively (Ref. 14). From Eq. (61), and noting that

$$n_p = \pi d_D^2 q \quad (62)$$

one obtains $K_p = \pi q_{\max}$.

Electrostatic mechanisms have been shown experimentally to have a large effect on the magnitude of the force of adhesion between particles. This effect is much larger than

expected, assuming normal charge distributions, suggesting that the details of surface irregularities and non-uniform charge distributions at the contacting surface are not properly accounted for in existing theories.

5.2.3 Surface Films

When particles are suspended in a condensable vapor, a film of liquid develops on the surface. If the vapor pressure is near its saturated value, the force of adhesion between two spheres of equal diameter with smooth, clean surfaces is estimated to be

$$F_s = 2.2\sigma d_D \quad (63)$$

where σ is the surface tension of the liquid film. In practice, the force of adhesion decreases sharply below the value given by Eq. (63) if the vapor pressure is below 90 percent of its saturated value. Surface contaminants and the non-submergence of surface irregularities will also reduce the expected force of adhesion (Ref. 14).

5.2.4 Maximum Strength

The previous sections have outlined a number of important forces of adhesion which are responsible for the strength of an agglomerate. It is informative to consider the maximum force for each of the mechanisms. For example, in the case of Van der Waals force of attraction, the spheres are assumed to be perfectly smooth with a minimum distance of separation. This would correspond to roughly 10 \AA (equivalent to two molecular diameters) in Eq. (58) and 2000 \AA in Eq. (59). The remaining parameters necessary are the surface tension ($\sigma = 72\text{ dynes/cm}$ for water at standard conditions) and the electron surface charge density. For the latter value, we choose 20 electrons as the average charge resulting from static electrification on a $1\text{-}\mu\text{m}$ particle (Ref. 19). It is understood, however, that the total charge could increase significantly for larger particles or those particles exposed to large concentrations of unipolar ions. Substitution of these values into Eqs. (58), (59), (60), and (63) provides expected values for the adhesion force on a $1\text{-}\mu\text{m}$ particle, and these are listed in Table 5.

It is apparent from Table 5 that in the absence of a limiting charge on perfectly smooth spheres, either Van der Waals, electrostatic, or surface tension mechanisms can determine the force of adhesion. Exposure of the spheres to large concentrations of ions of a single sign (unipolar charging) may produce very large electrostatic forces. Moreover, surface irregularities may alter the results shown in Table 5. Experimental measurements are necessary to resolve the question in specific applications.

**Table 5. Maximum Force of Adhesion between Two
Smooth Spheres of 1- μ m Diameter**

<u>Mechanism</u>	<u>Force (dynes)</u>
Van der Waals	$F_{v1} = 10^{-2}$, $a = 10 \text{ \AA}$ $F_{v2} = 1.25 \times 10^{-10}$, $a = 2000 \text{ \AA}$
Electrostatic	$F_e = 2.4 \times 10^{-2}$, 20 electrons $a = 10 \text{ \AA}$
Surface film	$F_s = 1.6 \times 10^{-2}$, $\gamma = 72 \text{ dynes/cm}$

5.3 STRENGTH OF ZnO AGGLOMERATES

Because of uncertainties associated with the simple theories of particle adhesion presented in Section 5.2, experimental data are usually necessary to predict the conditions for agglomerate breakup. In this section, we discuss the measured strength of a metal oxide agglomerate held together by Van der Waals forces. These results may be applicable to the aluminum oxide agglomerate known to exist in rocket motor plumes (Ref. 3) and used in the seeding of the gas flow in high-speed wind tunnels for purposes of measurement of gas velocity by laser doppler velocimetry (Ref. 20).

Meissner *et al.* (Ref. 20) placed ZnO powder of constituent particle size $d_p = 0.13$ and $0.26 \mu\text{m}$ in a rotating drum. Mesh sizes in the range from 0.25 to 1 mm were used, and the powder was tumbled for various time periods to produce agglomerates of known size and volume fraction of solids. The crushing strength of the powder was determined by placing the material between microscope slides and measuring the force which caused failure, as indicated by a reduction in spacing between the plates.

The results of Meissner's measurements have been replotted onto a single curve by the appropriate choice of the function represented on the abscissa of Fig. 18. Figure 18 indicates that in the absence of large amounts of water vapor (i.e., high relative humidity), the strength of the adhesive force F within the ZnO agglomerates is proportional to the constituent particle size (d_p). This suggests that Van der Waal's forces are the mechanism of adhesion for the ZnO agglomerates. The dependence of the strength of the agglomerate on the solid fraction (ϕ) is stronger, however, than the expected form presented by Rumpf in Eq. (57). One would also expect the force of failure of a single agglomerate to be higher than the measured value in Fig. 17, since a void existed between the agglomerates in the testing procedure of Meissner.

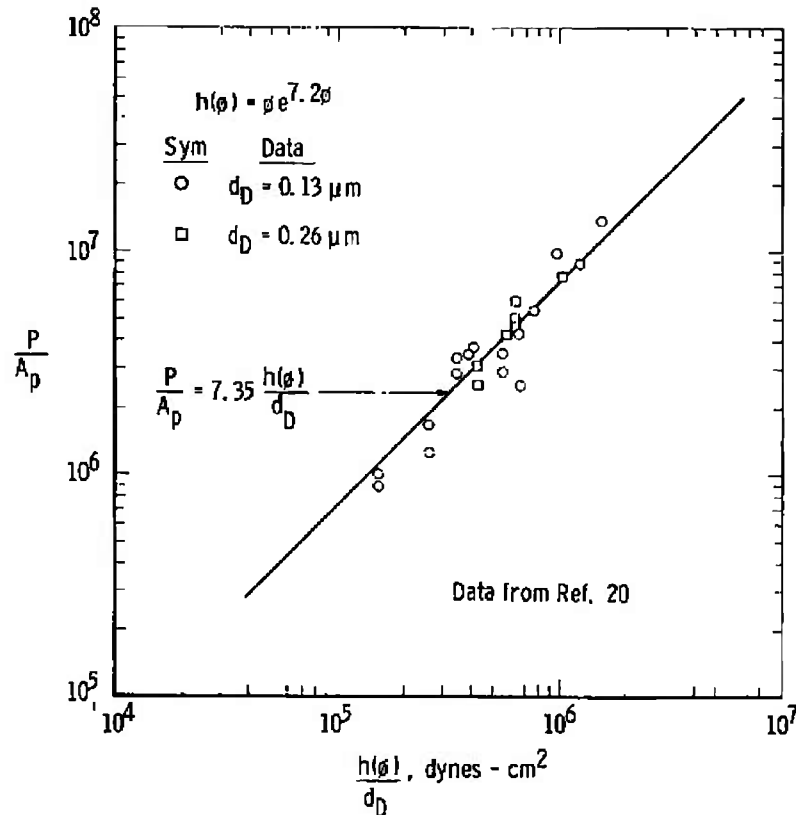


Figure 18. Crushing strength of ZnO agglomerates.

5.4 STRENGTH OF LIQUID DROPLETS

Uniform liquid spherical droplets are held together by surface tension forces. Since surface tension (σ) has units of force per unit length, the strength of the droplet p is thus the product of σ and the circumference or

$$p = \sigma \pi d \quad (64)$$

Writing Eq. (64) in the form of Eq. (57), one obtains a strength per unit cross-sectional area of the droplet, or

$$\frac{p}{A_p} = \frac{4\sigma}{d} \quad (65)$$

Caveny and Gany (24) have studied the breakup of molten Al/Al₂O₃ droplets in accelerating flow fields. Droplet breakup in these experiments was characterized in terms of the Weber number representing the ratio of inertial to surface tension forces. Droplet distortion is typically noted at a Weber number of 4, and breakup occurs in the range from 12 to 20. The latter values were slightly smaller than the values measured by Caveny and

Gany. If one assumes a drag coefficient of approximately 2.0 in the experiments of Caveny and Gany, for the particle inertial force given by Eq. (13), droplet distortion occurs when the drag per unit cross-sectional area of the droplet equals the surface tension strength given by Eq. (65). Breakup occurs, however, when the drag force is about four times the droplet strength.

5.5 CRITERIA FOR PARTICLE AND ZnO BREAKUP

From the foregoing, we are now in a position to establish criteria for particle breakup. The discussion is restricted to the possibility of breakup behind normal shocks. We hypothesize that the onset of particle breakup occurs when the drag force exceeds either the agglomerate or droplet strength, or when the Weber number (Wb) is greater than unity.

$$Wb = \frac{D}{P} > 1 \quad (66)$$

where D is given by Eq. (49) and the particle strength (P) by Eq. (57) or (65). In Eq. (57) the constituent particle adhesive force (F) which appears in P is given by either Eq. (58), (59), (60), or (63). Equation (66) is the same argument used to predict droplet breakup and the definition of a droplet Weber number.

Substituting for particle drag and strength in Eq. (66), the following criteria are established for each of the adhesive mechanisms discussed in Section 5.2. The criteria for liquid droplet breakup discussed in Section 5.4 is also included for completeness. Thus, particle breakup is expected to occur for the conditions listed below.

Van der Waals:

$$Wb = \frac{d_D P_0 C_{DG}(M_1)}{B k_1(\phi)} > 1 \quad (67)$$

where

$$B = B_1/a^2, \quad a < 2000 \text{ \AA}$$

$$B = B_2/a^3, \quad a > 2000 \text{ \AA}$$

$$k_1(\phi) = \phi/(1 - \phi)$$

Electrostatic:

$$Wb = \frac{P_0 C_{DG}(M_1)}{\epsilon q^2 k_3(\phi)} > 1 \quad (68)$$

where

$$k_3 = 3.1\pi k_1(\phi)$$

Surface films:

$$Wb = \frac{d_D P_o C_D g(M_1)}{\gamma k_2(\phi)} > 1 \quad (69)$$

where

$$k_2(\phi) = 2.17k_1(\phi)$$

Liquid droplets:

$$Wb = \frac{d P_o C_D g(M_1)}{4\sigma} > 1 \quad (70)$$

Equations (67), (68), and (69) indicate that the likelihood of particle breakup increases significantly as the volume fraction of solids (ϕ) decreases. Larger gas stagnation pressures (P_o) or constituent particle sizes (d_D) also contribute to agglomerate breakup. Moreover, the product $C_D g(M_1)$ in Figs. 15 and 16 increases with smaller agglomerate sizes (d). Thus, we can conclude that larger, more closely packed agglomerates made up of smaller constituent particles will have a greater tendency to resist breakup for a given set of gas stagnation conditions and shock Mach number than will smaller agglomerates made up of the same size particles.

It is instructive to consider the results of the experimental measurements of the strength of ZnO agglomerates (Ref. 20). Assuming a typical range of values of 2×10^5 dynes/cm² < $h(\phi)/dD < 2 \times 10^6$ dynes/cm² from Fig. 18, one would expect breakup to occur when the drag force exceeds these values. From Table 4, we consider an agglomerate of size $d = 10$ μ m flowing in a channel with a stagnation pressure $P_o = 50$ psi and $M_1 = 2$. Since $P_o = 3.4 \times 10^6$ dynes/cm², and $d_{D0}/k = 280$, and $C_D g(M_1) \approx 0.5$ from Fig. 15, then $P_o C_D g(M_1) \approx 1.7 \times 10^6$. Thus, the Weber number is in the range $0.85 < Wb < 8.5$, and breakup may be possible in this case.

If the same 10- μ m ZnO agglomerate were suspended in a gas typical of rocket plumes with $P_o = 600$ psi, $\gamma = 1.16$, and $M_1 = 4$, we would find $d_{D0}/k = 5 \times 10^2$ from Table 4 and calculate $P_o C_D g(M_1) = 8.1 \times 10^6$ dynes/cm². Thus, the Weber number is in the range $2.0 < Wb < 20$, and breakup is much more likely to occur.

It should be noted, however, that the value of the Weber number marking the onset of particle breakup may be much larger than unity, as in the experiments of Caveny and Gany

(Ref. 21). Thus, the calculations above are only estimations and, of course, the Weber number would be considerably reduced in the transonic or hypersonic regimes.

6.0 SUMMARY AND RECOMMENDATIONS

In summary, the various phenomena which influence the integrity of particle samples obtained from blunt probes immersed in supersonic flow have been examined. The two main sources of bias were identified as the flow around the probe, which is complicated because of the bow shock off the probe, and the particle breakup possibly induced by passage of the particle agglomerates or droplets through the bow shock. The dimensionless parameters necessary for scaling these phenomena and establishing criteria were defined (particle Reynolds, Knudsen, Mach, Stokes, and Weber numbers) and their ranges determined for the application of sampling in rocket exhaust plumes. Expressions for particle collection efficiency were defined and the necessary experimental measurements identified. The breakup of agglomerated particles into smaller particles was examined in terms of the various types of binding forces. The only material for which such binding forces have been measured is zinc oxide. If the aluminum oxide from rocket exhausts has a similar binding force, then agglomerates may break up.

The principal benefit of this study is the definition of the problems to be solved and identification of the needed data. The prediction of a probe collection efficiency is much too complicated analytically to expect believable results; experimental measurements are necessary. The experiments, however, need not be over the entire range of variables since the scaling laws have been established by this study. In fact, a sub-scale experiment using a laboratory two-phase flow generator and probes on the order of 2-mm diameter rather than the 25-mm probes used in rocket exhausts should be quite acceptable. Such an experiment can be used to quantify most probe designs for collection efficiency.

The second area requiring experimentation is the agglomerate breakup. It is first necessary to make crushing strength experiments on aluminum oxide similar to those made on zinc oxide. In this experiment, an amount of material collected from a rocket exhaust is examined for size distribution and then placed between two microscope slides. The measurement consists of the weight required to produce a change in the spacing. This measurement should be followed by an experiment in which the effect of shock waves on particle size can be determined. Either a free jet Mach disc or a shock tube would be used for such an experiment.

Finally, it should be noted that further progress in this area is hinged on experimental efforts.

REFERENCES

1. "Development of an Automated EPA Method: 5 Stack Samples." Report No. AESO-161-1-75, Naval Environmental Protection Support Service, Naval Air Rework Facility, North Island, California, 1975.
2. Hermesen, R. W. "Aluminum Oxide Particle Size for Solid Rocket Motor Performance Prediction." Presented at AIAA 19th Aerospace Science Meeting, St. Louis, Missouri, 1981.
3. Clark, M. S., Fisher, S. C. and French, E. P. "The Flow of Very Small Alumina Particles in a Solid Rocket Plume." Presented at AIAA/SAE/ASME 17th Joint Propulsion Conference, Colorado Springs, Colorado, 1981.
4. Liepmann, H. W. and Roshko, A. *Elements of Gasdynamics*. John Wiley, New York, 1957.
5. Shapiro, A. H. *The Dynamics and Thermodynamics of Compressible Fluid Flow*. Ronald Press Co., New York, 1953.
6. Forney, L. J. "Aerosol Impactor for Large Sample Volumes." *Review of Scientific Instruments*, Vol. 10, 1976, pp. 1264-1269.
7. McFarland, A. R., Ortiz, C. A. and Bertch, R. W., Jr. "Particle Collection Characteristics of a Single-Stage Dichotomous Sampler." *Environmental Science & Technology*, Vol. 12, No. 6, June 1978, pp. 679-682.
8. Friedlander, S. K. *Smoke Dust and Haze: Fundamentals of Aerosol Behavior*. John Wiley, New York, 1976.
9. Vincenti, W. G. and Kruger, C. H., Jr. *Introduction to Physical Gas Dynamics*. John Wiley, New York, 1965.
10. Carlson, D. J. and Hoglund, R. F. "Particle Drag and Heat Transfer in Rocket Nozzles." *AIAA Journal*, Vol. 2, No. 11, November 1964, pp. 1980-1984.
11. Crowe, C. T. "Drag Coefficient of Particles in a Rocket Nozzle." *AIAA Journal*, Vol. 5, No. 5, May 1967, pp. 1021-1022.

12. Miller, E. "Alumina Particle Velocity and Temperature in a Solid Rocket Plume." *AIAA Journal*, Vol. 13, No. 12, December 1975, pp. 1668-1670.
13. Serafini, J. S. "Impingement of Water Droplets on Wedges and Double-Wedge Airfoils at Supersonic Speeds." NACA Report No. 1159, 1954, p. 1159.
14. Davies, C. N., Ed. *Aerosol Science*. Academic Press, New York, 1966.
15. Fenton, D. L. "Turbine Engine Particulate Emission Characterization." Report No. FAA-RD-76-141, IIT Research Institute, Chicago, Illinois, September 1976.
16. Forney, L. J., Ravenhall, D. G. and Lee, S. S. "Theoretical and Experimental Study of a Two-Dimensional Virtual Impactor." *Environmental Science & Technology*, Vol. 16, No. 8, August 1982, p. 492.
17. Jeans, J. *An Introduction to the Kinetic Theory of Gases*. The University Press, Cambridge, England, 1940.
18. Rumpf, H. "Mechanics of Granules." *Chemie-Ingenieur-Technik*, Vol. 30, No. 3, 5 March 1958, pp. 144-158.
19. Kunkel, W. B. "The Static Electrification of Dust Particles on Dispersion into a Cloud." *Journal of Applied Physics*, Vol. 21, August 1950, pp. 820-832.
20. Meissner, H. P., Michaels, A. S., and Kaiser, R. "Crushing Strength of Zinc Oxide Agglomerates." *I&EC: Process Design and Development*, Vol. 3, No. 3, July 1964, pp. 202-205.
21. Caveny, L. H. and Gany, A. "Breakup of AL/AL₂O₃ Agglomerates in Accelerating Flow Fields." *AIAA Journal*, Vol. 17, No. 12, December 1979, pp. 1368-1371.

NOMENCLATURE

A	Cross-sectional area of probe ($= \pi L^2/4$) (cm ²)
A _E	Area of nozzle exit plane (cm ²)
A _p	Cross-sectional area of particle ($= \pi d^2/4$) (cm ²)
A _T	Area of nozzle throat (cm ²)

a	Distance of separation between constituent particles (cm)
B₁	Van der Waals constant (ergs)
B₂	Van der Waals constant (erg-cm)
b	Reference value in Sutherland's equation ($\text{gm-cm}^{-1}\text{-sec}^{-1}\text{-}^{\circ}\text{K}^{-1/2}$)
C	Slip correction factor
C_D	Drag coefficient
c	Speed of sound (cm-sec^{-1})
D	Particle drag behind shock (dynes)
d	Particle diameter (cm)
d_D	Constituent particle diameter (cm)
F	Force of adhesion (dynes)
f₁	Dimensionless function proportional to particle Stokes number
f₂	Dimensionless function proportional to particle Knudsen number behind shock
f₃	Particle Mach number ($= M_{p2}$) behind shock
f₄	Dimensionless function proportional to local particle Reynolds number behind shock
f₅	Dimensionless function proportional to particle Reynolds number Re_p
f₆	Dimensionless function proportional to particle stopping distance for non-Stokesian particles ($Re_p > 1$)
k	Constant in particle groups ($= b/r^{1/2}$) (gm-cm^{-2})
k_B	Boltzmann's constant ($\text{gm-cm}^2\text{-sec}^{-2}\text{-}^{\circ}\text{K}^{-1}$)

Kn	Particle Knudsen number behind shock
K_p	Limit of surface charge density (coul⁻cm⁻²)
L	Probe diameter (cm)
M	Gas Mach number
M_p	Particle Mach number
m	Molecular mass (gm)
m_p	Particle mass (gm)
n	Particles per unit cross-sectional area (cm⁻²)
n_s	Particles per unit mass in sample probe (gm⁻¹)
n_m	Particles per unit mass in mainstream (gm⁻¹)
p	Particle strength (dynes)
P_{1,2}	Gas pressures (dynes-cm⁻²)
q	Surface charge density (coul⁻cm⁻²)
q_m	Mass flow rate in mainstream in probe area (gm-sec⁻¹)
q_s	Mass flow rate in probe sample line (gm-sec⁻¹)
R	Specific gas constant (cm²-sec⁻²-°K⁻¹)
Re	Local particle Reynolds number behind shock
Re_p	Particle Reynolds number
Re_L	Probe Reynolds number
St	Particle Stokes number

T	Gas temperature ($^{\circ}\text{K}$)
T_g	Gas Temperature near particle ($^{\circ}\text{K}$)
T_p	Particle temperature ($^{\circ}\text{K}$)
T_0	Sutherland's constant ($^{\circ}\text{K}$)
t	Time (sec)
u, v, w	Components of particle and fluid velocities in three orthogonal directions (cm-sec^{-1})
\vec{v}	Particle velocity (cm-sec^{-1})
\vec{v}_f	Gas velocity (cm-sec^{-1})
\vec{v}^+	Normalized particle velocity ($= \vec{v}/v_1$)
\vec{v}_f^+	Normalized gas velocity ($= \vec{v}_f/v_1$)
Wb	Particle Weber number
z	Particle coordination number

Greek Symbols

γ	Ratio of specific heats
δ	Shock detachment distance (cm)
ϵ	Coulomb's law constant ($\text{dynes-cm}^2\text{-coul}^{-1}$)
Θ	Normalized time ($= v_1 t/L$)
λ	Gas near free path (cm)
μ	Gas viscosity ($\text{gm-cm}^{-1}\text{-sec}^{-1}$)
ρ	Gas density (gm-cm^{-3})

ρ_p	Particle density (gm-cm^{-3})
σ	Surface tension (dynes-cm^{-1})
ϕ	Solid fraction (agglomerate)
ω	Defined function of Re

Subscripts

1	Upstream of shock
2	Downstream of shock
o	Stagnation conditions
r	Reference
f	Fluid